Article

Developmental Cell

BCKDK regulates the TCA cycle through PDC in the absence of PDK family during embryonic development

Graphical abstract

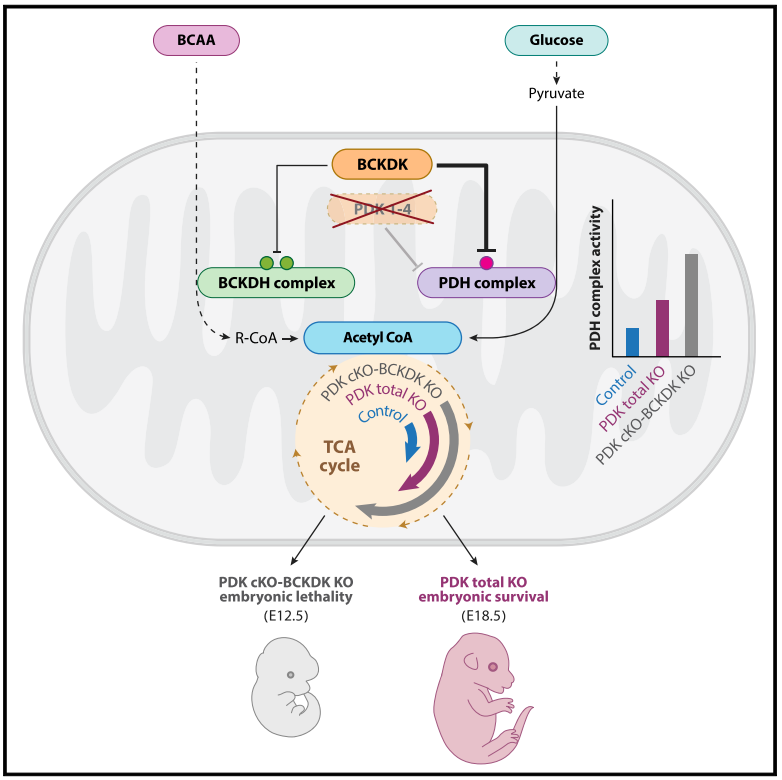

Highlights

- Deletion of all four *Pdk* genes did not cause embryonic lethality
- Deletion of *Bckdk* and *Pdk* family prevented PDC phosphorylation and increased its activity
- This resulted in increased pyruvate entry into the TCA cycle and embryonic lethality
- This compensatory mechanism directly connects between BCAA and glucose catabolic pathways

Authors

Lia Heinemann-Yerushalmi, Lital Bentovim, Neta Felsenthal, ..., Sergey Malitsky, Ayelet Erez, Elazar Zelzer

Correspondence

eli.zelzer@weizmann.ac.il

In brief

Heinemann-Yerushalmi et al. show that, upon deletion of all four *Pdk* genes, mouse embryos developed to term and PDC remained phosphorylated. By contrast, deletion of *Bckdk* and *Pdk* family led to the loss of PDC phosphorylation, increased PDC activity and pyruvate entry into the TCA cycle, and embryonic lethality.

Heinemann-Yerushalmi et al., 2021, Developmental Cell *56*, 1182–1194
April 19, 2021
https://doi.org/10.1016/j.devcel.2021.03.007

CellPress

CellPress

Developmental Cell

Article

BCKDK regulates the TCA cycle through PDC in the absence of PDK family during embryonic development

Lia Heinemann-Yerushalmi,[1,6] Lital Bentovim,[1,6] Neta Felsenthal,[1] Ron Carmel Vinestock,[1] Nofar Michaeli,[1] Sharon Krief,[1] Alon Silberman,[5] Marina Cohen,[2] Shifra Ben-Dor,[3] Ori Brenner,[2] Rebecca Haffner-Krausz,[2] Maxim Itkin,[4] Sergey Malitsky,[4] Ayelet Erez,[5] and Elazar Zelzer[1,7,*]

[1]Department of Molecular Genetics, Weizmann Institute of Science, Rehovot 7610001, Israel
[2]Department of Veterinary Resources, Weizmann Institute of Science, Rehovot 7610001, Israel
[3]Bioinformatics and Biological Computing Unit, Biological Services, Weizmann Institute of Science, Rehovot, 76100, Israel
[4]Department of Life Sciences Core Facilities, Weizmann Institute of Science, Rehovot 7610001, Israel
[5]Department of Biological Regulation, Weizmann Institute of Science, Rehovot 7610001, Israel
[6]These authors contributed equally
[7]Lead contact
*Correspondence: eli.zelzer@weizmann.ac.il
https://doi.org/10.1016/j.devcel.2021.03.007

SUMMARY

Pyruvate dehydrogenase kinases (PDK1–4) inhibit the TCA cycle by phosphorylating pyruvate dehydrogenase complex (PDC). Here, we show that PDK family is dispensable for murine embryonic development and that BCKDK serves as a compensatory mechanism by inactivating PDC.
First, we knocked out all four *Pdk* genes one by one. Surprisingly, *Pdk* total KO embryos developed and were born in expected ratios but died by postnatal day 4 because of hypoglycemia or ketoacidosis.
Moreover, PDC was phosphorylated in these embryos, suggesting that another kinase compensates for PDK family. Bioinformatic analysis implicated branched-chain ketoacid dehydrogenase kinase (*Bckdk*), a key regulator of branched-chain amino acids (BCAAs) catabolism. Indeed, knockout of *Bckdk* and *Pdk* family led to the loss of PDC phosphorylation, an increase in PDC activity and pyruvate entry into the TCA cycle, and embryonic lethality. These findings reveal a regulatory crosstalk hardwiring BCAA and glucose catabolic pathways, which feed the TCA cycle.

INTRODUCTION

The pyruvate dehydrogenase complex (PDC) plays a major role as the gatekeeper that links glycolysis to the tricarboxylic acid (TCA) cycle, maintaining metabolic balance and energy production through the rate-limiting and physiologically irreversible oxidative decarboxylation of pyruvate (Harris et al., 2002). Owing to its importance, PDC regulation has been extensively studied since its discovery in the late 1960s (Tracy et al., 1968). The regulatory mechanism was shown to involve reversible phosphorylation by intrinsic regulatory enzymes, a family of pyruvate dehydrogenase kinases (PDKs) 1–4 (Wieland, 1983). These isoenzymes phosphorylate and inactivate PDC on three serine residues of its catalytic E1α subunit (PDH1a), namely, S293 (site 1), S300 (site 2), and S232 (site 3). Studies of site specificity showed that all four PDKs phosphorylate site 1 and site 2, whereas site 3 is phosphorylated only by PDK1. However, phosphorylation of any of the three serine residues leads to complete inactivation of PDC activity (Korotchkina and Patel, 1995).

PDK activity blocks the flux of pyruvate into the TCA cycle, which results in a metabolic shift to glycolysis for energy production. PDC activity is regulated by *Pdk* family in a short- and long-term manner (Jeoung, 2015). In the short term, several allosteric regulators can activate PDK according to the levels of end products, namely, increased acetyl-CoA/coenzyme A ratio and reduced and oxidized nicotinamide adenine dinucleotide ($NADH/NAD^+$) ratio (Garland et al., 1964). In the long term, the amount of PDK protein is determined by different physiological conditions and in a tissue-specific manner (Bowker-Kinley et al., 1998; Kolobova et al., 2001; Sugden and Holness, 2006; Roche and Hiromasa, 2007). This involves transcriptional and translational regulation via hormonal regulators, such as estrogen receptor and glucocorticoid receptor (Jeong et al., 2012), and transcription factors, such as oxygen sensor hypoxia inducible factor 1 subunit alpha (HIF1α) (Aragonés et al., 2009; Kim et al., 2006; Kluza et al., 2012; Lu et al., 2008; Papandreou et al., 2006; Prigione et al., 2014; Semenza, 2009). HIF1α regulation of *Pdk* was shown to occur in cancer cells, which prefer to maintain anaerobic metabolism even in the presence of oxygen, a phenomenon known as the Warburg effect or aerobic glycolysis (Stacpoole, 2017). Here, the increase in glycolysis supplies intermediates for branching pathways that synthesize the

macromolecules necessary for cell proliferation (Tennessen et al., 2014). Based on these studies, *Pdk* family and specifically PDK1 became a specific target for anticancer drug development (Jeoung, 2015; Saunier et al., 2016). In addition to its role in cancer, the HIF1-PDK axis is also vital for mammalian embryonic development (Dunwoodie, 2009; Koh and Powis, 2012; Simon and Keith, 2008). For example, during endochondral bone formation, HIF1α is required for various processes in the hypoxic growth plate (Amarilio et al., 2007; Hallmann et al., 1987; Maes et al., 2012; Provot et al., 2007; Schipani et al., 2001), one of which is to directly regulate the expression of *Pdk1*(Bentovim et al., 2012).

Extensive studies on the involvement of the *Pdk* family in metabolic regulation have provided some indications for functional redundancy among its members. Cell culture experiments showed redundancy between PDK1 and PDK2 (Dunford et al., 2011), whereas loss-of-function studies in mice lacking *Pdk2*, *Pdk4*, or even both revealed no major effect (Jeoung et al., 2012). Nevertheless, the question of the necessity of the four PDK isoenzymes and the functional redundancy among them has yet to be addressed by a direct genetic approach.

In this study, we investigated the requirement of Pdk's for embryonic development using the hypoxic growth plate as a model. Strikingly, mouse strains of double, triple, and eventually quadruple KO, that is, mice lacking all four *Pdk* genes, displayed normal skeletal development and were born in the expected Mendelian ratios. These results suggest that the entire *Pdk* family is dispensable for embryogenesis. Moreover, we show that, in the absence of all PDK isoenzymes, PDC is still phosphorylated, implying the existence of a backup mechanism. Bioinformatic analysis implicated branched-chain ketoacid dehydrogenase kinase (BCKDK), an enzyme that regulates the catabolism of branched-chain amino acids (BCAAs), in this mechanism. The loss of PDC phosphorylation and consequent increases in PDC activity and pyruvate entry into the TCA cycles, which we observed in mice and cell lines lacking all *Pdk*'s and *Bckdk*, strongly support this possibility. Overall, we identify BCKDK regulation of PDC as a mechanism that can backup PDK family function during embryonic development.

RESULTS

PDK1, PDK2, and PDK4 are dispensable for development and growth

To study *in vivo* the role of PDK family, we first focused on PDK1. Because the involvement of this isoenzyme in metabolic homeostasis was mostly studied in the context of cells under hypoxic conditions (Kim et al., 2006; Papandreou et al., 2006; Prigione et al., 2014; Semba et al., 2016), we chose the hypoxic growth plate during mouse bone development as a model (Amarilio et al., 2007; Bentovim et al., 2012; Maes et al., 2012; Provot et al., 2007; Provot and Schipani, 2005). Using the knockout (KO)-first allele method, we generated 3 mouse strains: floxed-*Pdk1*, *Pdk1-lacZ* KO, and *Pdk1* KO (Figure S1A). Examination of the *Pdk1-lacZ* KO reporter line verified strong *Pdk1* expression in developing bones of E14.5 embryos, including long bones, vertebrae, and facial bones (Figures S1B and S1C). Surprisingly, both homozygous *Pdk1-lacZ* KO and *Pdk1* KO mice had no apparent bone phenotype during embryonic development, as confirmed by skeletal preparation (Figures 1A and 1B) and histological sections (Figures 1C and 1D). These mice produced viable and fertile colonies matching expected Mendelian ratios (Figure 1G).

To understand the lack of phenotype, we examined the levels of different metabolites related to the TCA and glycolysis pathways in growth plate chondrocytes from *Pdk1* KO and control mice. Chondrocytes from tibiofemoral growth plates were extracted and grown in cell culture, and the TCA and glycolysis intermediates were examined. Results showed similar levels of metabolites (glucose, glutamine, and glutamate) in control and *Pdk1* KO chondrocytes, indicating that metabolic homeostasis in those cells is maintained. Moreover, we detected similar levels of lactate, suggesting that a metabolic shift to enhanced glycolysis occurred in the absence of *Pdk1* (Figure 1F).

A plausible explanation for the lack of phenotype in the absence of *Pdk1* is that other PDK isoenzymes compensated for its activity. Null mutants for *Pdk2* and *Pdk4* were reported to develop normally and have viable and fertile colonies (Dunford et al., 2011; Jeoung et al., 2006). Therefore, to examine the functional redundancy hypothesis, we generated double KO (dKO) and triple KO (tKO) mouse models lacking *Pdk1* and *Pdk2* or *Pdk1* and *Pdk4* or all 3 of these genes. The loss of these genes was verified by quantitative reverse transcription polymerase chain reaction (qRT-PCR) (Figure S2A). Surprisingly, none of the combinations exhibited any bone phenotype (Figures 1H–1M). Moreover, *Pdk* tKO mice produced viable and fertile colonies matching expected Mendelian ratios (Figure 1N). These outcomes indicated that PDK1, PDK2, and PDK4 are dispensable for bone and embryonic development.

Loss of the *Pdk* family results in postnatal lethality owing to hypoglycemia and ketoacidosis

The lack of phenotype in the *Pdk* tKO mice led us to study the only remaining candidate from the *Pdk* family, namely, *Pdk*3. Recently, *Pdk*3 was also shown to be a HIF1α target under hypoxic conditions (Prigione et al., 2014). Thus, we hypothesized that *Pdk*3 might be sufficient to maintain embryonic development. To test this hypothesis, we established a genetic model in which the expression of all 4 *Pdk* genes is deleted. Considering the possible embryonic lethality, we sought to delete *Pdk3* on the background of an intact *Pdk1* using $Pdk1^{flox/flox}$ allele combined with *Pdk2* and *Pdk4* KO. By crossing these mice with a specific Cre line, we could remove *Pdk1* in a tissue-specific manner and, thereby, prevent early lethality. For that purpose, we utilized the CRISPR/Cas9 method to target *Pdk3* gene on the genetic background of *Prx1-Cre*;$Pdk1^{flox/null}Pdk2^{-/-}Pdk4^{-/-}$ mice and generated 2 independent lines. The first was the quadruple conditional KO (cKO) *Prx1-Cre*;$Pdk1^{flox/flox}Pdk2^{-/-}Pdk3^{-/-}Pdk4^{-/-}$ mice, which lack all 4 *Pdk* genes in *Prx1*-expressing limb mesenchyme lineages only. The second line was back-crossed to generate $Pdk1^{-/-}Pdk2^{-/-}Pdk3^{-/-}Pdk4^{-/-}$ quadruple KO mice (total KO) (Figure 2A).

Using qRT-PCR and western blot analysis on *Pdk* total KO mice, we verified deletion of all 4 *Pdk* genes at both mRNA and protein levels (Figures 2B and 2C). Moreover, western blot analysis of chondrocytes derived from *Pdk* cKO growth plates showed deletion of PDK1 protein compared with cells from wild-type (WT) and control littermates, where *Prx1-Cre* was not

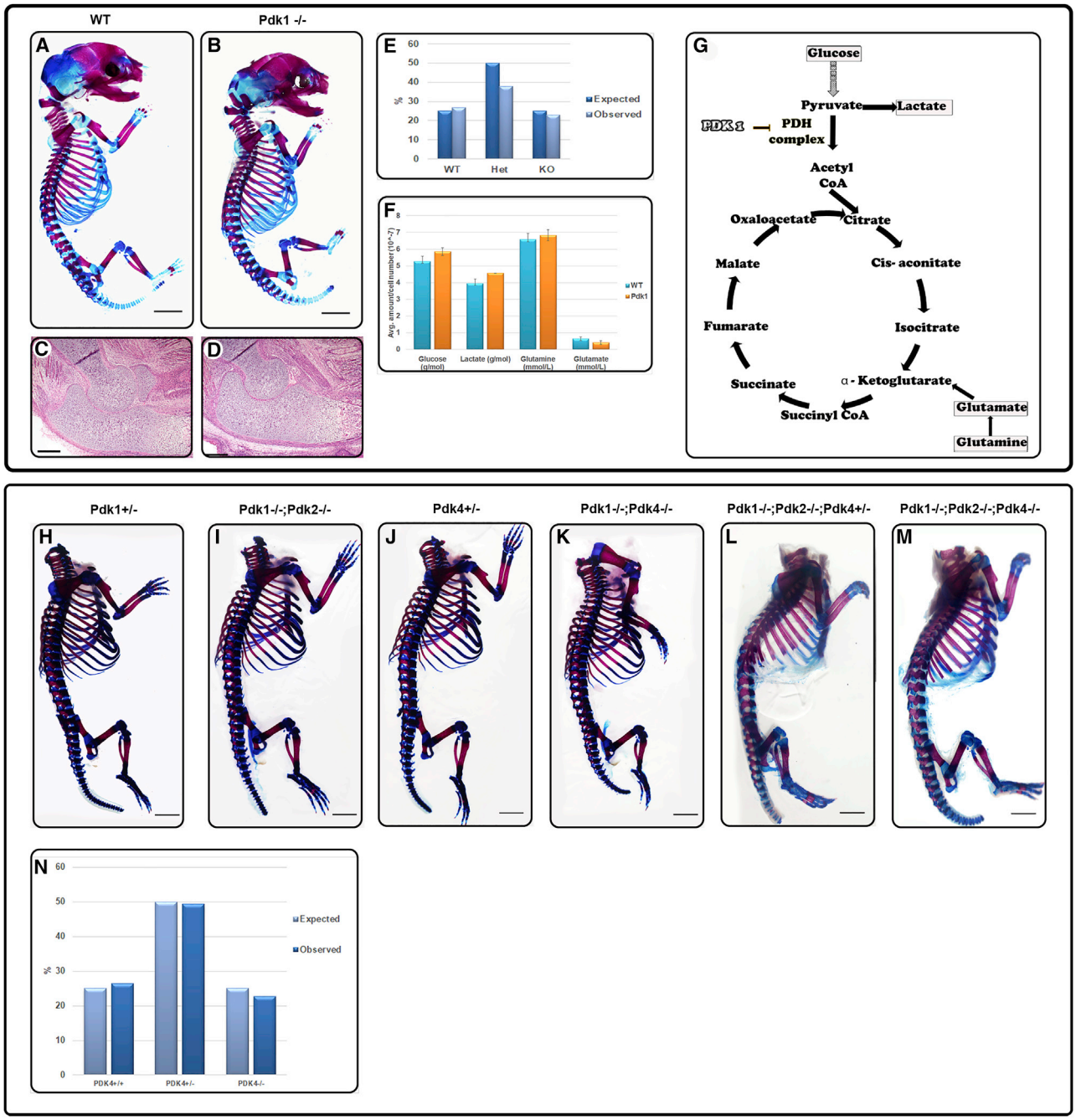

Figure 1. Deletion of single, double, or triple *Pdk* genes *in vivo* does not affect embryonic development

(A and B) Skeletal preparations of control (A) and *Pdk1* KO (B) E17.5 embryos showing no skeletal phenotype (scale, 50 μm).

(C and D) H&E staining of control and *Pdk1* KO E15.5 embryonic sections of olecranon and distal humerus growth plates (scale, 50 μm).

(E) Graph showing expected Mendelian ratios of *Pdk1* KO progeny (n = 56, from three different colonies).

(F) Graph showing similar absolute levels of glycolysis-TCA pathway-related metabolites in chondrocytes from E17.5 *Pdk*1 KO and WT embryos (Nova analyzer, n = 3; data are presented as mean ± SD).

(G) Schematic illustration of the TCA cycle highlights the entry point of relevant metabolites.

(H–M) Skeletal preparations of control (*Pdk1*$^{+/-}$, H), *Pdk1-Pdk2* dKO (I), control (*Pdk4*$^{+/-}$, J) and *Pdk1-Pdk4* dKO (K), control (Pdk1$^{-/-}$Pdk2$^{-/-}$ *Pdk4*$^{+/-}$, l), and *Pdk1-Pdk2-Pdk4* tKO (M) newborn pups. (H and I, J and K, and L and M are littermates; scale, 50 μm).

(N) Graph showing expected Mendelian ratios in colonies of *Pdk* tKO mice (n = 114, from 4 different colonies).

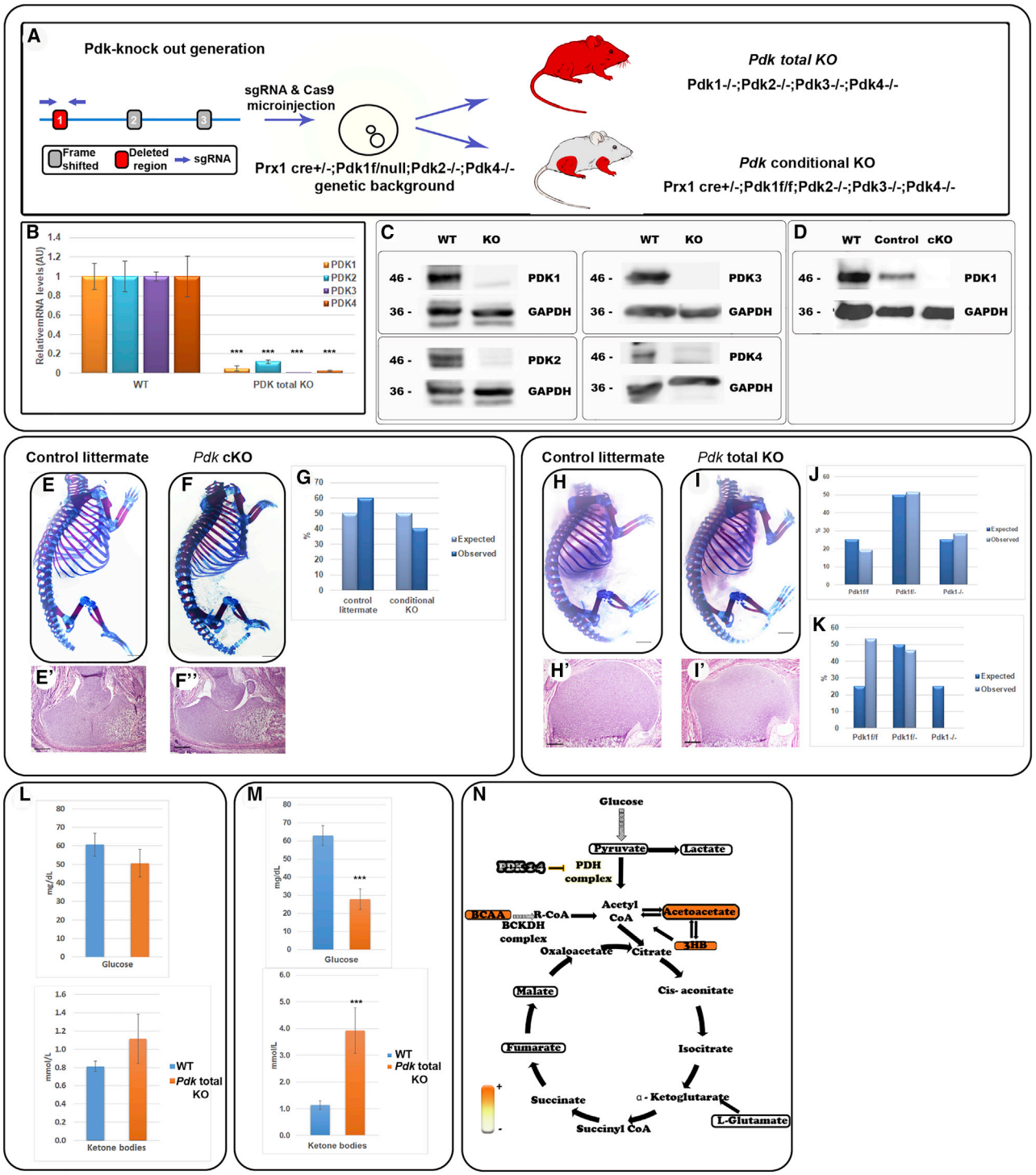

Figure 2. Deletion of the entire *Pdk* family results in postnatal lethality

(A) Schematic representation of *Pdk3* gene and the targeted site of CRISPR-Cas9-mediated deletion. This was followed by zygote injection to generate *Pdk* total KO mice or *Pdk* cKO in limb mesenchyme only, depending on the genetic background.

(B) qRT-PCR of *Pdk1-4* mRNA confirms deletion of all four genes, as compare to WT (***p < 0.0001; n = 4 for each genotype; data are normalized to *Tbp* and presented as mean ± SD).

(C) Protein expression analysis (western blot) of four PDK isoenzymes in heart samples derived from *Pdk* total KO or WT P0 pups shows complete deletion of the entire PDK family (representative images, n = 3).

(D) Western blotting of chondrocytes from *Pdk* cKO, control littermate, and WT embryos shows deletion of PDK1 in the mutant (representative images, 3 biological repeats, n = 5 for each sample).

(legend continued on next page)

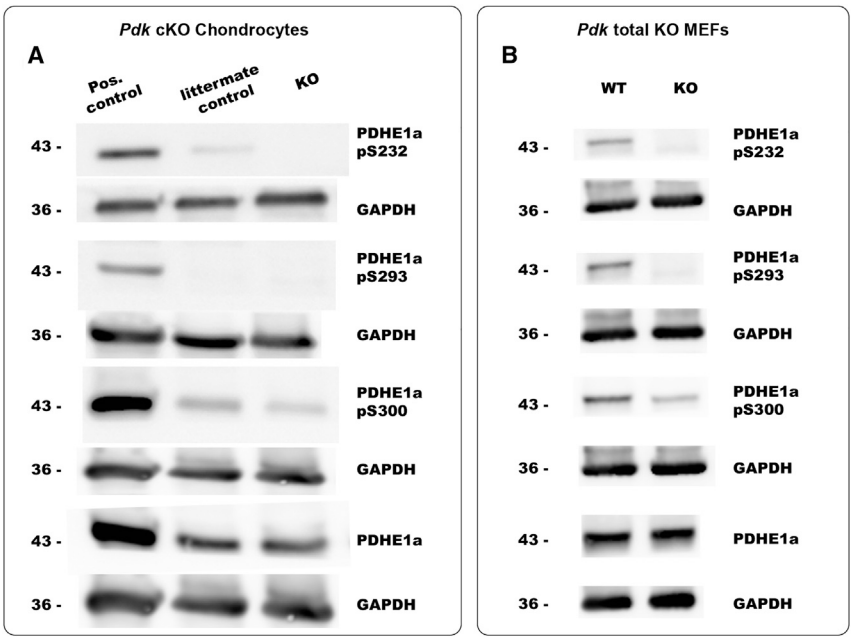

Figure 3. PDC phosphorylation is PDK-independent

(A and B) Western blot analysis of the three PDC phosphorylation sites in chondrocytes extracted from growth plates of E17.5 *Pdk* cKO embryos (A; *Prx1-CrePdk1*$^{flox/flox}$*Pdk2*$^{-/-}$*Pdk3*$^{-/-}$*Pdk4*$^{-/-}$) and MEFs derived from *Pdk* total KO embryos (B), compared with WT. As controls, PDH1a and endogenous GAPDH total protein levels were measured. Each chondrocyte sample is a pool of 5 biological repeats; n = 3 for all groups. Hearts of E17.5 WT embryos are shown as a positive control; control littermates were *Prx1-Cre*-negative. MEF samples, n = 7.

present (Figure 2D). The results indicated effective deletion of all 4 *Pdk* genes in both total KO and cKO mice. Surprisingly, skeletal preparation and histological sections from *Pdk* cKO mice revealed no bone phenotype (Figures 2E–2F′). By monitoring the colonies, we found that *Pdk* cKO mice produced viable and fertile colonies matching expected Mendelian ratios (Figure 2G). Similarly, the examination of bone development in skeletal preparation and histological sections of *Pdk* total KO embryos revealed no major skeletal phenotype (Figures 2H–2I′). However, although embryonic Mendelian ratios were observed as expected (Figure 2J), this mouse strain did not produce viable offspring, as shown by the non-Mendelian ratios of mature mice (Figure 2K).

Examination of newborn *Pdk* total KO pups revealed that they died between P0 and P4. To determine the cause of death, we analyzed histological sections from adrenal gland, brain, brown fat tissue, heart, kidney, liver, lung, small intestines, and spinal cord of E18.5 embryos. The examination revealed no major anatomical abnormalities (Figure S3).

A previous study showed that *Pdk* loss results in high utilization of glucose, followed by elevation of ketone bodies (Jeong et al., 2012). Therefore, we examined blood levels of glucose and ketone bodies as a possible cause of lethality. As observed in Figures 2L and 2M, although at E18.5 no differences were observed between WT and *Pdk* total KO embryos, P1 *Pdk* total KO pups displayed significantly higher levels of 3-β−hydroxybutyrate (3HB), a common ketone body, and lower glucose levels than WT pups (Figure 2M).

Deeper metabolic profiling of serum composition in these pups showed significantly low levels of pyruvate and lactate together with a higher utilization of acetyl-CoA, reflected by higher levels of the ketone bodies acetoacetate and 3HB, reduced production of more distal TCA metabolites, and high levels of BCAAs (Figure 2N). These results are consistent with the expected effect of *Pdk* loss (Crabb and Harris, 1979; Jeoung et al., 2012) and suggest that the cause of the early postnatal death was ketoacidosis and hypoglycemia. Altogether, these results suggest that *Pdk* family is dispensable for embryonic development but is necessary postnatally to maintain energy metabolic balance.

PDC phosphorylation is maintained upon PDK family loss of function

To gain molecular insight into the viability of *Pdk* total KO embryos, we studied the 3 phosphorylation sites on PDH1a subunit, which regulate PDC activity. First, we examined by western blot analysis PDC phosphorylation sites in chondrocytes isolated from growth plates of *Pdk* cKO embryos, which lack all *Pdk* genes in limb mesenchyme lineages. Interestingly, we found that one of the three sites, namely, S300, was phosphorylated (Figure 3A). To rule out the possibility that the phosphorylation of site S300 resulted from PDK1 contamination by surrounding tissues, such as skeletal muscles, we produced mouse embryonic fibroblasts (MEFs) from the total *Pdk* KO mice. As seen in

(E and F′) Skeletal preparations (E and F) and H&E-stained olecranon and distal humerus sections (E′ and F′) from E18.5 *Prx1-Cre*;*Pdk1f*$^{f/f}$;*Pdk2*$^{-/-}$;*Pdk3*$^{-/-}$;*Pdk4*$^{-/-}$ embryos and control littermates (without Cre) show that the *Pdk* cKO embryos develop normally (scale, 100 μm).

(G) Graph showing Mendelian ratios of genotypes in *Pdk* cKO progeny (n = 45, from 4 different colonies).

(H and I′) Skeletal preparations at E18.5 (H and I) and H&E-stained sections (H′,I′) from P0 *Prx1-Cre*;*Pdk1*$^{f/-}$;*Pdk2*$^{-/-}$;*Pdk3*$^{-/-}$;*Pdk4*$^{-/-}$ mice and control littermates (scale, 100 μm).

(J) Graph showing Mendelian ratios of genotypes in E18.5 *Pdk* total KO embryos (n = 102 embryos, from 16 different litters).

(K) Graph showing non-Mendelian ratios of genotypes in *Pdk* total KO mature mice, as a result of loss of the total KO genotype (n = 47, from 4 different colonies).

(L and M) Graphs showing *in utero* blood levels of glucose and 3HB, a ketone body, in *Pdk* total KO E18.5 embryos and P1 pups (M), compared with WT. Data are presented as mean ± SE (embryos: n_{WT} = 9, n_{KO} = 6; P1: n_{WT} = 9; n_{KO} = 4, from 3 independent litters; $p < 0.05$, Student's t test).

(N) Scheme of serum metabolic profiles of P1 *Pdk* total KO pups, as determined by LC-MS polar metabolite analysis. Higher levels are shown in orange and lower levels in yellow compared with WT levels ($p < 0.05$; fold change of >2, n_{WT} = 4; n_{KO} = 3).

Figure 3B, site S300 was phosphorylated in these MEFs as well. To strengthen the observation that the phosphorylation is maintained upon the loss of the *Pdk* family, we examined PDC phosphorylation in other tissues such as heart, lungs, and kidney of *Pdk* total KO embryos. As seen in Figure S4, in all tested tissues, PDC was phosphorylated on at least one site in a tissue-specific manner. Altogether, these results suggest the existence of a backup mechanism that phosphorylates and inactivates PDC in the absence of all four PDKs.

Bckdk is necessary for embryonic development in the absence of *Pdk* family

Our results suggested that another kinase, which is not a PDK, phosphorylates PDH1a subunit of PDC. To identify this kinase, we searched for suitable candidates using bioinformatic tools, such as Ensemble (Paten et al., 2008) and GeneCards (Stelzer et al., 2016). One candidate that emerged was *Bckdk*, which catalyzes the phosphorylation and inactivation of the branched-chain α-ketoacid dehydrogenase complex (BCKDC), the key regulatory enzyme of the valine, leucine, and isoleucine catabolic pathways (Broquist and Trupin, 1966). GenesLikeMe analysis (Stelzer et al., 2009) predicted that *Bckdk* was a paralog of *Pdk1* and belonged to the same mitochondrial kinase proteins family, mainly by sequence and domain similarity (Figure 4A). Moreover, protein-protein interaction analysis by STRING (Szklarczyk et al., 2017) predicted BCKDK to interact with PDH1a subunit of PDC (Figure 4B).

Based on these observations, we hypothesized that BCKDK serves as the backup mechanism for PDK family during embryonic development by regulating PDC phosphorylation to inhibit its activity. To test this hypothesis, we sought to delete *Bckdk* on *Pdk* family KO genetic background. *Bckdk* KO mice were previously reported to be viable at neonatal stages and to display growth retardation only at three weeks of age (Joshi et al., 2006). To avoid embryonic lethality, we opted to delete *Bckdk* on the background of *Pdk1* cKO combined with *Pdk2-4* KO. Thus, we used the CRISPR-Cas9 method to generate a*Prx1-Cre-Pdk1*$^{flox/null}$*Pdk2*$^{-/-}$*Pdk3*$^{-/-}$*Pdk4*$^{-/-}$*Bckdk*$^{-/-}$ mouse strain (Figure 4C). The deletion of *Bckdk* gene was verified at both mRNA and protein levels by qRT-PCR and western blotting, respectively (Figures 4D and 4E). Crossing *Prx1-Cre-Pdk1*$^{flox/null}$*Pdk2*$^{-/-}$*Pdk3*$^{-/-}$*Pdk4*$^{-/-}$*Bckdk*$^{+/-}$ to *Pdk1*$^{flox/null}$*Pdk2*$^{-/-}$*Pdk3*$^{-/-}$*Pdk4*$^{-/-}$*Bckdk*$^{+/-}$ mice, we generated 3 strains: *Prx1-Cre-Pdk1*$^{flox/flox}$*Pdk2*$^{-/-}$*Pdk3*$^{-/-}$*Pdk4*$^{-/-}$*Bckdk*$^{-/-}$, *Prx1-Cre-Pdk1*$^{flox/null}$*Pdk2*$^{-/-}$*Pdk3*$^{-/-}$*4*$^{-/-}$*Bckdk*$^{-/-}$, and *Pdk1*$^{flox/null}$*Pdk2*$^{-/-}$*Pdk3*$^{-/-}$*Pdk4*$^{-/-}$*Bckdk*$^{+/-}$.

First, we examined the viability of embryos lacking *Pdk1* in limb mesenchyme lineages and null for *Pdk2*, *Pdk3*, *Pdk4*, and *Bckdk*. For that, we crossed *Prx1-Cre-Pdk1*^{floxflox}*Pdk2*$^{-/-}$*Pdk3*$^{-/-}$*Pdk4*$^{-/-}$*Bckdk*$^{+/-}$ mice with *Pdk1*^{floxflox}*Pdk2*$^{-/-}$*Pdk3*$^{-/-}$*4*$^{-/-}$*Bckdk*$^{+/-}$ and analyzed genotype distribution between E10.5 and E12.5, a stage at which *Prx1-Cre* is activated (Logan et al., 2002) (Figure 4F). Results showed that, at E10.5 and E11.5, the numbers of *Prx1-Cre-Pdk1*^{floxflox}*Pdk2*$^{-/-}$*Pdk3*$^{-/-}$*Pdk4*$^{-/-}$*Bckdk*$^{-/-}$ embryos were close to the expected Mendelian ratios. However, some of these embryos displayed developmental retardation in comparison with control littermates (Figure 4G). By contrast, at E12.5 the prevalence of this genetic combination was lower than expected, indicating embryonic lethality (Figure 4F). Moreover, we failed to observe this combination postnatally (Figure 4H).

To study genetic interaction between *Pdk1* and *Bckdk*, we crossed *Pdk1*$^{flox/null}$*Pdk2*$^{-/-}$*Pdk3*$^{-/-}$*Pdk4*$^{-/-}$*Bckdk*$^{+/-}$ mice with *Pdk1*$^{flox/null}$*Pdk2*$^{-/-}$*Pdk3*$^{-/-}$*Pdk4*$^{-/-}$*Bckdk*$^{+/-}$ mice. As seen in Figure 4I, in the presence of an intact *Pdk1* gene, all 3 combinations of *Bckdk*, namely, WT, heterozygous, and null, were observed. In contrast, heterozygosity of both *Pdk1* and *Bckdk* resulted in 50% reduction from the expected ratio, and no *Pdk1*$^{flox/null}$*Pdk2*$^{-/-}$*Pdk3*$^{-/-}$*Pdk4*$^{-/-}$*Bckdk*$^{-/-}$ offspring were observed, suggesting genetic interaction between these genes.

Together, these results clearly suggest that the loss of *Bckdk* on *Pdk* family KO background results in embryonic lethality and strongly support the hypothesis that BCKDK compensates for the absence of PDK isoenzymes during development.

BCKDK regulates PDC phosphorylation and activity and pyruvate entry into the TCA cycle

To further validate our hypothesis, we proceeded to test directly whether *Bckdk* is necessary for the phosphorylation of PDC subunit PDH1a in the absence of all *Pdk* family members. To overcome the early embryonic lethality of mice lacking all *Pdk* genes and *Bckdk*, we used *Pdk1*$^{flox/flox}$*Pdk2*$^{-/-}$*Pdk3*$^{-/-}$*Pdk4*$^{-/-}$*Bckdk*$^{-/-}$ embryos to generate primary MEF cultures. Next, we infected these cells with adeno-Cre virus to ablate the expression of *Pdk1* or with adeno-GFP as a control. As seen in Figure 5A, upon infection with adeno-Cre, concomitantly with the reduction in PDK1 expression, PDH1a phosphorylation on site S300 was reduced compared with control cells; however, some phosphorylation was still noticeable. Because we observed low levels of PDK1 expression in adeno-Cre infected cells, we inhibited the activity of the remaining PDK1 by supplementing the culture with dichloroacetate (DCA), a PDK inhibitor (Stacpoole, 1989). As seen in Figure 5A, DCA nearly eliminated the phosphorylation of site S300. These results provide strong molecular evidence to the ability of BCKDK to regulate PDC by phosphorylation.

To demonstrate the biochemical effect of this regulation, we next quantified PDC activity in cells lacking *Pdk* family and in cells lacking both *Pdk* family and *Bckdk*. First, we examined PDC activity in MEFs from WT or *Pdk* total KO embryos. As seen in Figure 5B, *Pdk* family loss resulted, as expected, in a significant 2-fold increase in PDC activity compared with WT cells. Next, we examined PDC activity in our primary *Pdk1*$^{flox/flox}$*Pdk2*$^{-/-}$*Pdk3*$^{-/-}$*Pdk4*$^{-/-}$*Bckdk*$^{-/-}$ MEFs, which also lack *Bckdk*. Although in control MEFs infected with adeno-GFP virus (*Pdk* cKO-*Bckdk* KO GFP), which retain *Pdk1* expression, the increase in PDC activity was similar to the one observed in *Pdk* total KO cells, infection with adeno-Cre virus (*Pdk* cKO-*Bckdk* KO CRE) further increased the signal by 1.5 times relative to adeno-GFP infected MEFs and *Pdk* total KO-derived MEFs and by 3 times relative to the WT.

Next, to provide direct metabolic evidence to the consequences of the observed changes in PDC activity, we evaluated pyruvate entry to the TCA cycle by conducting metabolic tracing experiments on these primary cell lines. Using labeled [3-^{13}C]pyruvate, we measured the relative abundancies of metabolites (m), including the TCA cycle intermediates

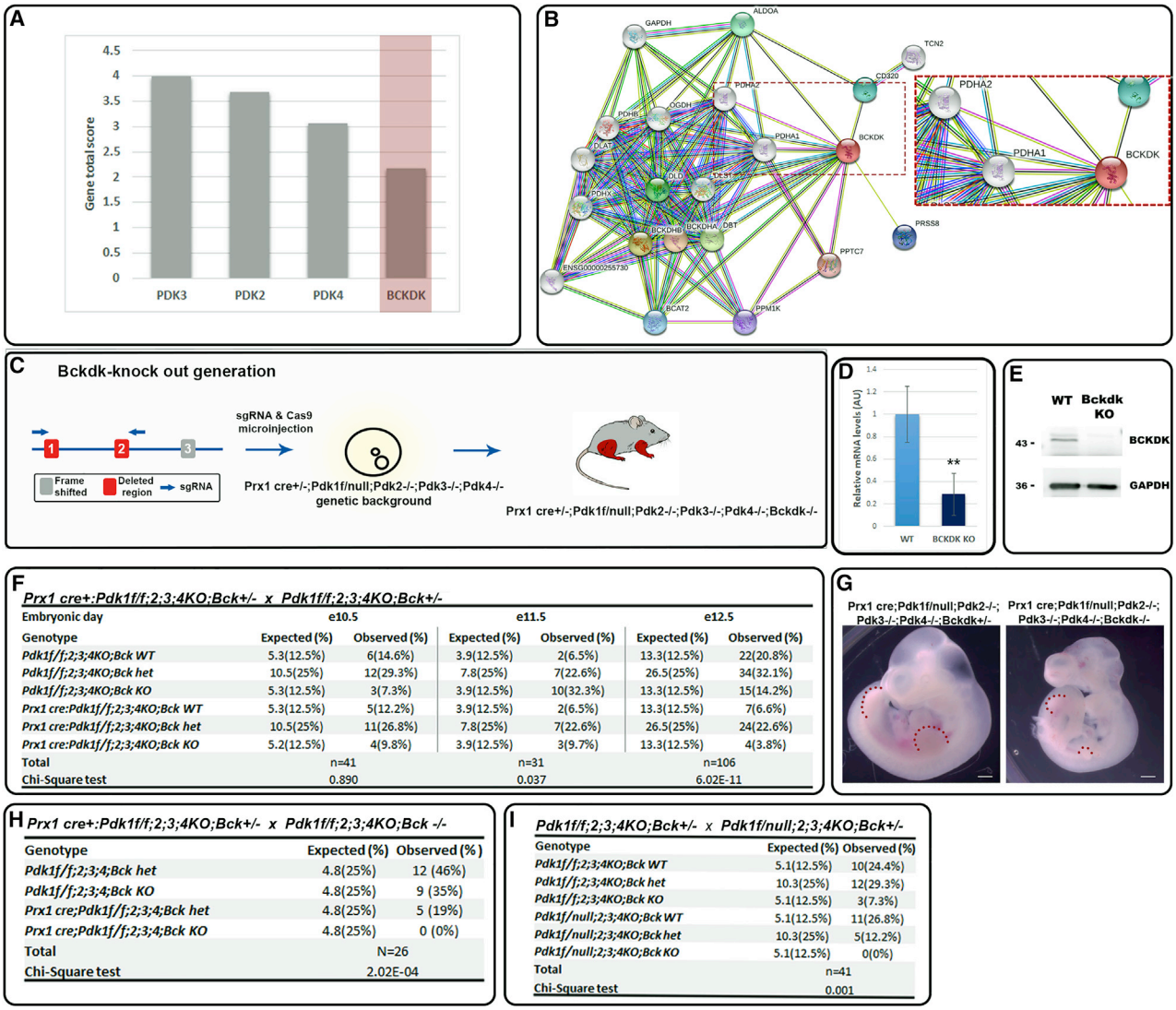

F *Prx1 cre+:Pdk1f/f;2;3;4KO;Bck+/- x Pdk1f/f;2;3;4KO;Bck+/-*

Embryonic day	e10.5		e11.5		e12.5	
Genotype	Expected (%)	Observed (%)	Expected (%)	Observed (%)	Expected (%)	Observed (%)
Pdk1f/f;2;3;4KO;Bck WT	5.3(12.5%)	6(14.6%)	3.9(12.5%)	2(6.5%)	13.3(12.5%)	22(20.8%)
Pdk1f/f;2;3;4KO;Bck het	10.5(25%)	12(29.3%)	7.8(25%)	7(22.6%)	26.5(25%)	34(32.1%)
Pdk1f/f;2;3;4KO;Bck KO	5.3(12.5%)	3(7.3%)	3.9(12.5%)	10(32.3%)	13.3(12.5%)	15(14.2%)
Prx1 cre:Pdk1f/f;2;3;4KO;Bck WT	5.3(12.5%)	5(12.2%)	3.9(12.5%)	2(6.5%)	13.3(12.5%)	7(6.6%)
Prx1 cre:Pdk1f/f;2;3;4KO;Bck het	10.5(25%)	11(26.8%)	7.8(25%)	7(22.6%)	26.5(25%)	24(22.6%)
Prx1 cre:Pdk1f/f;2;3;4KO;Bck KO	5.2(12.5%)	4(9.8%)	3.9(12.5%)	3(9.7%)	13.3(12.5%)	4(3.8%)
Total	n=41		n=31		n=106	
Chi-Square test	0.890		0.037		6.02E-11	

G

H *Prx1 cre+:Pdk1f/f;2;3;4KO;Bck+/- x Pdk1f/f;2;3;4KO;Bck -/-*

Genotype	Expected (%)	Observed (%)
Pdk1f/f;2;3;4;Bck het	4.8(25%)	12 (46%)
Pdk1f/f;2;3;4;Bck KO	4.8(25%)	9 (35%)
Prx1 cre;Pdk1f/f;2;3;4;Bck het	4.8(25%)	5 (19%)
Prx1 cre;Pdk1f/f;2;3;4;Bck KO	4.8(25%)	0 (0%)
Total	N=26	
Chi-Square test	2.02E-04	

I *Pdk1f/f;2;3;4KO;Bck+/- x Pdk1f/null;2;3;4KO;Bck+/-*

Genotype	Expected (%)	Observed (%)
Pdk1f/f;2;3;4KO;Bck WT	5.1(12.5%)	10(24.4%)
Pdk1f/f;2;3;4KO;Bck het	10.3(25%)	12(29.3%)
Pdk1f/f;2;3;4KO;Bck KO	5.1(12.5%)	3(7.3%)
Pdk1f/null;2;3;4KO;Bck WT	5.1(12.5%)	11(26.8%)
Pdk1f/null;2;3;4KO;Bck het	10.3(25%)	5(12.2%)
Pdk1f/null;2;3;4KO;Bck KO	5.1(12.5%)	0(0%)
Total	n=41	
Chi-Square test	0.001	

Figure 4. *Prx1-CrePdk* cKO-*Bckdk* KO mice display embryonic lethality

(A) GenesLikeMe analysis identifies *Bckdk* as a *Pdk1* paralog, along with the other *Pdk* family members (total score combines sequences, domains, super pathways, expression, compounds, and gene ontology similarities).

(B) STRING analysis predicts protein-protein interaction between BCKDK and PDH complex subunit PDH1a (string legend: yellow, textmining; black, co-expression; pink, experimentally determined).

(C) Schematic representation of *Bckdk* gene and the targeted sites of CRISPR/Cas9-mediated deletion. This was followed by zygote injection to generate *Prx1-Cre-Pdk1*$^{flox/null}$*Pdk2*$^{-/-}$*Pdk3*$^{-/-}$*Pdk4*$^{-/-}$*Bckdk*$^{-/-}$ mouse, lacking *Pdk1* in limb mesenchyme lineages.

(D) qRT-PCR of *Bckdk* mRNA in *Prx1-Cre-Pdk1*$^{flox/null}$*Pdk2*$^{-/-}$*Pdk3*$^{-/-}$*Pdk4*$^{-/-}$*Bckdk*$^{-/-}$ mice, compare with WT (**$p < 0.001$; $n = 3$ for each genotype; data normalized to *Tbp* and presented as mean ± SD).

(E) Protein expression analysis by western blotting shows complete deletion of BCKDK in *Pdk1*$^{flox/flox}$*Pdk2*$^{-/-}$*Pdk3*$^{-/-}$*Pdk4*$^{-/-}$*Bckdk*$^{-/-}$ MEF cells ($n = 3$).

(F) Expected Mendelian ratios and observed genotype distribution of *Prx1-Cre-Pdk1*^{floxflox}*Pdk2*$^{-/-}$*Pdk3*$^{-/-}$*4*$^{-/-}$*Bckdk*$^{+/-}$ crossed with *Pdk1*^{floxflox}*Pdk2*$^{-/-}$*Pdk3*$^{-/-}$*Pdk4*$^{-/-}$*Bckdk*$^{+/-}$ embryos at E10.5 ($n = 41$), E11.5 ($n = 31$), and E12.5 ($n = 106$).

(G) Representative E10.5 *Prx1-Cre-Pdk1*^{floxflox}*Pdk2*$^{-/-}$*Pdk3*$^{-/-}$*Pdk4*$^{-/-}$*Bckdk*$^{-/-}$ embryo displays delayed development compared with control *Bckdk* heterozygous littermate (dashed red lines indicate the limbs; scale, 50 μm).

(H and I) Mendelian ratios and genotype distributions of *Prx1-Cre-Pdk1*^{floxflox}*Pdk2*$^{-/-}$*Pdk3*$^{-/-}$*Pdk4*$^{-/-}$*Bckdk*$^{+/-}$ crossed with *Pdk1*^{floxflox}*Pdk2*$^{-/-}$*Pdk3*$^{-/-}$*Pdk4*$^{-/-}$*Bckdk*$^{-/-}$ mice and (I) *Pdk1*$^{flox/null}$*Pdk2*$^{-/-}$*Pdk3*$^{-/-}$*Pdk4*$^{-/-}$*Bckdk*$^{+/-}$ crossed with *Pdk1*$^{flox/null}$*Pdk2*$^{-/-}$*Pdk3*$^{-/-}$*Pdk4*$^{-/-}$*Bckdk*$^{+/-}$ mice (postnatal stage, after weaning). Data are presented as numbers and percentage of the total progeny; statistical significance was determined by chi-square test.

citrate, α-ketoglutarate, succinate and fumarate, malate and oxaloacetate, and their m+2 and m+3 mass isotopomers (Table S1). The level of m+2 isotopomers indicates activation of the PDC pathway (pyruvate decarboxylation), whereas activation of the pyruvate carboxylase (PC) pathway is indicated by m+3 isotopomers (pyruvate carboxylation).

As seen in Figure 5C, the m+2 mass isotopomer fraction of labeled intermediates increased significantly in *Pdk* total KO

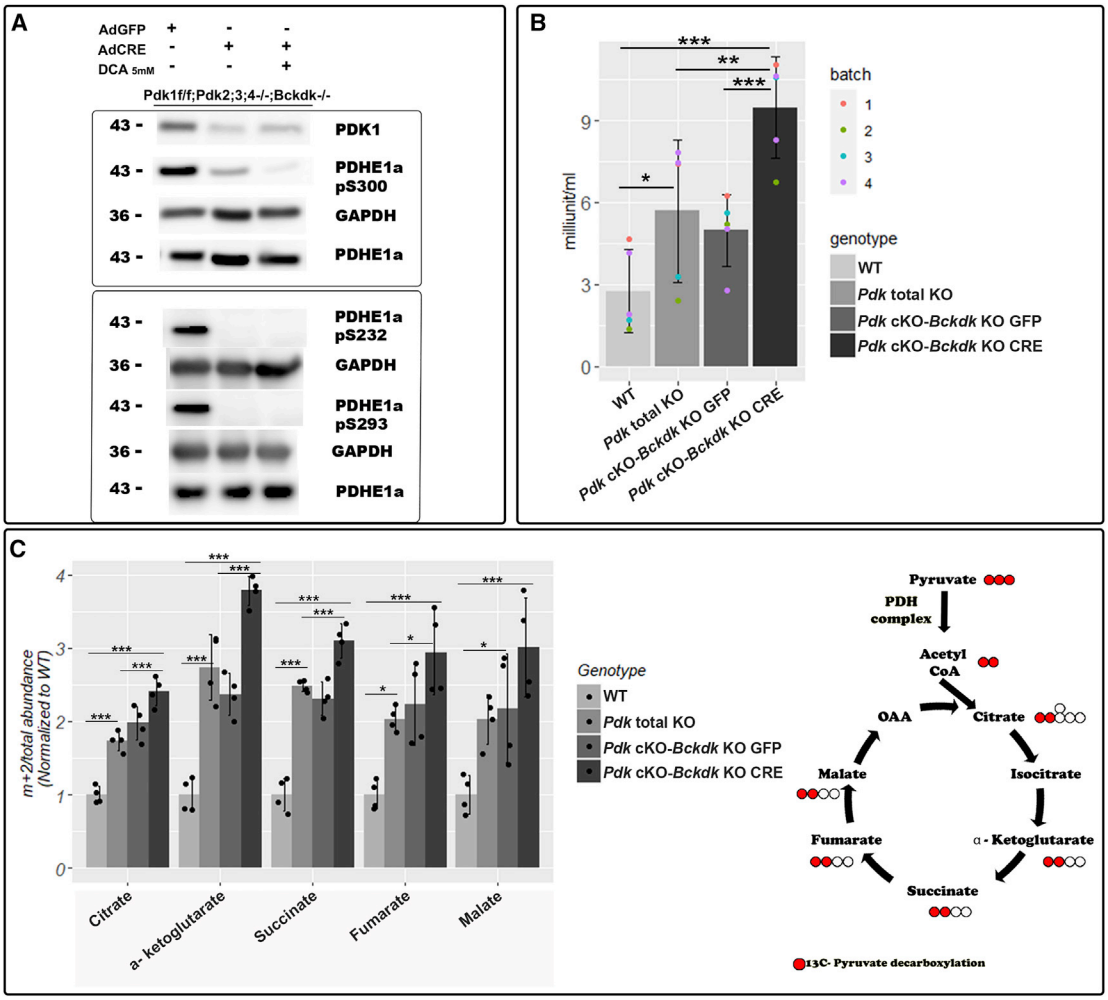

Figure 5. PDC phosphorylation and activity is BCKDK dependent

(A) Western blot of PDK1 and of PDH1a phosphorylated sites pS300, the main active PDC site in MEFs, pS232 and pS293 in MEFs derived from *Pdk1*$^{flox/flox}$ *Pdk2*$^{-/-}$*Pdk3*$^{-/-}$*Pdk4*$^{-/-}$*Bckdk*$^{-/-}$ mice infected with either adeno-GFP as a control, or adeno-CRE with or without addition of 5 mM DCA, to ablate PDK1 (representative images, n = 6 from 2 different sets of experiments).

(B) PDC activity assay in MEFs from *Pdk* total KO or *Pdk1*$^{flox/flox}$*Pdk2*$^{-/-}$*Pdk3*$^{-/-}$*Pdk4*$^{-/-}$*Bckdk*$^{-/-}$ mice infected with either adeno-GFP (*Pdk* cKO-*Bckdk* KO GFP) or adeno-Cre (*Pdk* cKO-*Bckdk* KO CRE), and WT as a control (mean ± SD, ***p < 0.001, **p < 0.01, *p < 0.05, n = 5 for each genotype from 4 different experiments, ANOVA multiple comparison test).

(C) Metabolic tracing analysis of [3-^{13}C]pyruvate entry into the TCA cycle using LC-MS. MEFs from *Pdk* total KO, *Pdk1*$^{flox/flox}$*Pdk2*$^{-/-}$*Pdk3*$^{-/-}$*Pdk4*$^{-/-}$*Bckdk*$^{-/-}$ or WT mice were infected with either adeno-GFP (*Pdk* cKO-*Bckdk* KO GFP) or adeno-Cre (*Pdk* cKO-*Bckdk* KO CRE). Graph shows the relative abundancies of m+2 mass isotopomers of TCA cycle intermediates from the total abundance of these metabolites, normalized to WT levels. On the right is a schematic of the TCA cycle showing the labeled metabolites (mean ± SD, ***p < 0.001, **p < 0.01, *p < 0.05, n = 4 for each genotype, ANOVA multiple comparison test). Total abundance equals the sum of m, m+2, and m+3 mass isotopomers.

MEFs relative to WT cells. Predictably, upon deletion of *Pdk* family and *Bckdk* (*Pdk* cKO-*Bckdk* KO CRE), the fractions of these metabolites further increased compared with both GFP control (*Pdk* cKO-*Bckdk* KO GFP) and *Pdk* total KO MEFs. By contrast, we failed to see any significant difference in m+3 mass isotopomer fractions of labeled intermediates, suggesting that the PC pathway is not affected by the loss of PDK and BCKDK enzymes (Figure S5). Collectively, these results provide strong molecular and biochemical evidence to the ability of BCKDK to regulate PDC phosphorylation and, thereby, activity.

DISCUSSION

The ability of cells to adapt to different environmental conditions and maintain energetic homeostasis is one of the hallmarks of life. Using oxygen as the most common electron acceptor allows cells to maximize utilization of acetyl-CoA driven from three catabolic pathways of glucose, amino acids, and fatty acids feeding the TCA cycle. In this work, we discover a regulatory metabolic circuit between glucose and BCAA catabolic pathway. We found that BCKDK, a key regulator of BCAA catabolic pathway, regulates the activity of PDC, the gatekeeper of the glucose catabolic

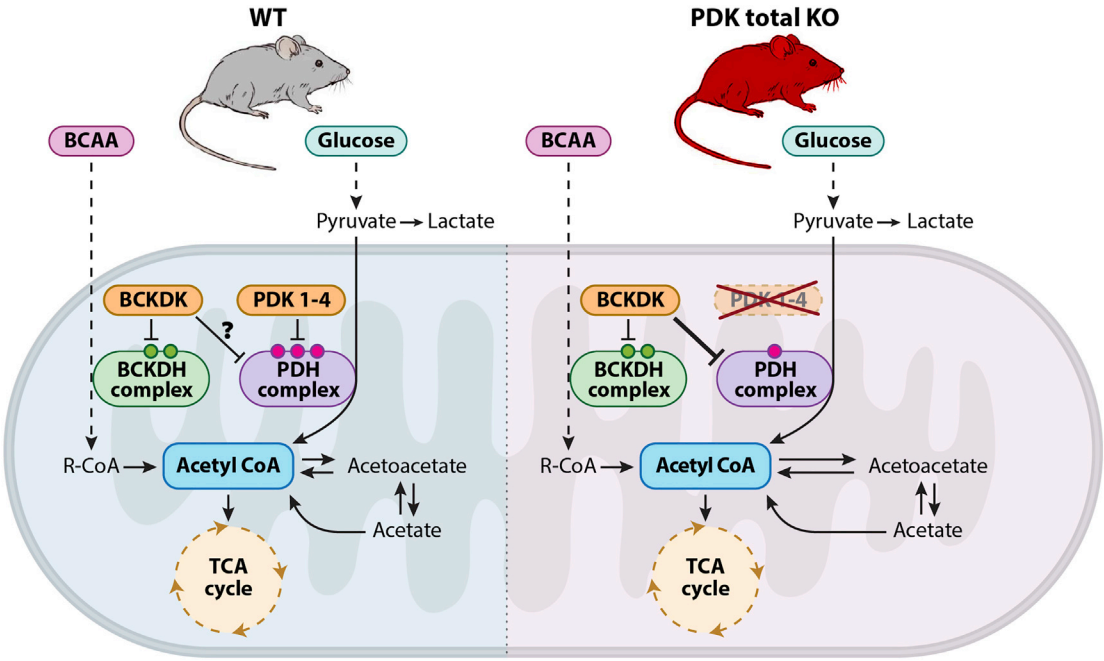

Figure 6. BCKDK compensates for *Pdk* loss of function via PDC phosphorylation

Cartoon depicting the interplay between glucose and BCAA catabolism in WT (left) versus *Pdk* total KO mice (right). In WT mice, PDC is inactivated by phosphorylation on 3 serine residues, whereas in the *Pdk* total KO mice, these phosphorylation sites are *Bckdk* dependent. This level of regulation implicates BCKDK as a functional paralog of the PDK family, which may also act in the same way in the presence of PDKs.

pathway. As the underlying mechanism, we show that BCKDK regulates PDC phosphorylation. This finding establishes BCKDK as a backup mechanism for the PDK family in regulating PDC activity, which allows cellular metabolic balance to sustain embryonic development (Figure 6).

BCAAs are a group of indispensable amino acids that includes leucine, isoleucine, and valine (Joshi et al., 2006). Their catabolism serves the cellular energetic balance by feeding the TCA cycle through a 2-step degradation pathway of transamination to form branched-chain α-keto acids (BCKAs), followed by oxidation and decarboxylation resulting in an irreversible synthesis of acetyl-CoA entering the TCA cycle (Zhang et al., 2017). The second step is crucial for degradation by BCKDC multienzyme. Therefore, BCKDC regulation is important to maintain proper levels of BCAAs and normal development (Joshi et al., 2006). Interestingly, PDC and BCKDC share many structural and enzymatic properties and mechanism of regulation. Similar to PDC, BCKDC is regulated by reversible phosphorylation of its E1 subunit on two serine sites (ser293 and ser303) mediated by its own native kinase, BCKDK. The activity of the entire BCKDC complex depends on BCKDK function, which is regulated by a feedback loop of substrate metabolites, for example, BCAA blood levels (Zhou et al., 2012).

Over the years, an interplay between the glucose and BCAA catabolic pathways has been established (Zhang et al., 2017). Recently, it was shown that these pathways can regulate one another through feedback loops of nutrients blood circulation, that is, glucose and amino acids, to maintain energetic balance. Excessive or insufficient levels of glucose or BCAAs were shown to influence transcription of elements of the parallel pathway. For example, BCAA levels can improve glucose uptake by up-regulation of glucose transporters (Nishitani et al., 2005), and a reciprocal effect was shown when high levels of glucose suppress the expression of BCAA degradation enzymes (Shao et al., 2018). Our discovery that BCKDK can phosphorylate PDC uncovers another level of regulation that hardwires glucose and BCAA degradation pathways through direct enzymatic regulation and not by a feedback loop of circulating nutrients.

From an evolutionary viewpoint, Oppenheim et al. (Oppenheim et al., 2014) recently showed that, in some parasites lacking mitochondrial PDC, acetyl-CoA is converted from pyruvate by BCKDC, which fulfills PDC function. Therein, it was suggested that BCKDC evolved earlier than PDC. Although the ancestral gene of the regulators of these complexes, that is, *Pdk* and *Bckdk*, is yet to be discovered, sequence similarities between *Pdk* and *Bckdk* have placed them as paralogs belonging to the same mitochondrial kinase family (Ferriero et al., 2013; Gudi et al. (1995); Popov et al. 1993 ; Wynn et al. (2000). Here, we provide strong *in vivo* evidence suggesting that *Bckdk* is not only a paralog but also a functional paralog of the *Pdk* family. One interesting question that remains is whether BCKDK acts only as a backup mechanism for the loss of the PDK family or is it a part of PDC regulation in normal conditions as well. Another intriguing question that is raised by the observed functional compensation is whether PDKs can compensate for the absence of BCKDK. This assumption makes sense considering that *Bckdk* KO mice are viable and exhibit growth retardation only at 3 weeks of age, owing to lack of BCKDC regulation (Joshi et al., 2006).

Another interesting point emerging from our finding that BCKDK can regulate PDC is the tissue-specific expression of

PDK isoenzymes (Gudi et al., 1995). Moreover, each isoenzyme was shown to be regulated by different physiological conditions (Jeoung, 2015; Sugden and Holness, 2006; Roche and Hiromasa, 2007). By contrast, several studies support the possibility of functional redundancy among PDK family members, for example, between PDK1 and PDK2 in muscle tissue *in vitro* (Dunford et al., 2011) and between PDK2 and PDK4 *in vivo* (Jeoung et al., 2012). Our failure to identify major developmental phenotype in embryos that lost different *Pdk* genes increases the scope of known functional redundancy among these 4 isoenzymes. The sequential targeting of these genes demonstrates that each PDK can compensate for the loss of the other family members. Another level of this complex regulation relates to the tightly controlled rate of PDC phosphorylation, which is maintained by the balance between the activity of PDK and pyruvate dehydrogenase phosphatases (PDPs). The latter are 2 enzymes that reverse PDK activity and thereby reactivate PDC (Huang et al., 1998). Given the importance of this balance, it is interesting to see whether the activity levels of PDKs and PDPs are regulated such that a reduction in PDK activity would lead to a concomitant reduction in PDP activity. Such coordination might contribute to the maintenance of PDC phosphorylation in the absence of PDK family. Overall, PDC regulation by kinase versus phosphatase activity should be further studied under different physiological conditions.

On that note, hypoxic conditions have long been associated with pathologies, such as tissue ischemia, inflammation, and cancer (Semenza, 2001). However, hypoxic microenvironments were shown to be essential for mammalian embryonic development (Dunwoodie, 2009). In either state, HIF1 transcription factor initiates a key molecular response that maintains O_2 homeostasis and metabolic balance (Papandreou et al., 2006; Simon and Keith, 2008). In particular, the HIF1α-PDK axis is considered a major regulator of cell adaptation to hypoxia by both controlling energy production and decreasing mitochondrial oxygen consumption (Aragonés et al., 2009; Kim et al., 2006; Kluza et al., 2012; Papandreou et al., 2006; Prigione et al., 2014; Semenza, 2009). However, our results of normal development in the absence of one side of this axis, namely, all PDKs, question its significance. There are 3 possibilities to reconcile our findings with the common view. One is that HIF1α activation of a wide range of downstream target genes is adaptive enough to support metabolic energy balance under hypoxia even without inactivation of PDC. For example, by activating pyruvate kinase isoform M2 (PKM2), which diverts pyruvate to the pentose phosphate pathway (Prigione et al., 2014). Second, it is possible that by activating another yet undescribed mechanism, HIF1α compensates for the absence of PDK family. In that context, the possibility that HIF1α can regulate *Bckdk* should be considered. Finally, it is possible that the involvement of HIF1α-PDK axis is restricted to the development or function of specific organs, which are dispensable for embryonic development. In support of this explanation is our finding that mice lacking all *Pdk* genes in limb mesenchyme developed normally, whereas total *Pdk* KO mice died at early neonatal stages. The metabolic abnormalities in these newborn total KO mice strongly imply that the affected organs are involved in physiological regulation of the organism, which is critical for its survival postnatally but not during embryogenesis. It is also possible that, during development, the consequences of metabolic abnormalities, such as ketone body accumulation and hypoglycemia, are buffered by the safe environment of the placenta (Weissgerber and Wolfe, 2006). Obviously, the different outcomes of embryonic development and postnatal growth of *Pdk* total KO mice do not exclude the possibility that these 2 processes have different metabolic requirements. In that case, it is possible that BCKDK could back up for PDKs only during the embryonic period. One point that remains unresolved is the early lethality of embryos lacking both PDK family and BCKDK in the Prx1 lineage, compared with the viability of embryos lacking either PDKs or BCKDK. It is possible that the loss of BCKDK and PDK family leads to severe metabolic disturbances that are ultimately fatal; however, this requires further investigation.

To conclude, our findings provide insight into the functional redundancy among PDK family members in modulating PDC activity to maintain energy production and cell survival, while revealing the existence of a previously unknown backup mechanism, which places *Bckdk* as a functional paralog of *Pdk*. This backup mechanism unveils a regulatory crosstalk between 2 central metabolic pathways that feed the TCA cycle. The finding of this backup mechanism may promote the development of therapeutic strategies for complex diseases involving changes in the metabolic state of cells, such as cancer, diabetes, and many other metabolic diseases.

Limitations

This work provides an *in vivo* model for PDK family functionality during murine embryonic development, which reveals a unique link between BCAA and glucose catabolism. Nevertheless, this model has several technical and conceptual limitations. First, *Pdk* total KO mice died between P0 and P4. Thus, extended physiological examination of individual mice was limited to a short time period, whereas embryonic examination should take into consideration placental protection. Second, loss of function of *Pdk* family along with *Bckdk* resulted in early embryonic lethality, even when *Pdk1* deletion was restricted to *Prx1* lineage. This limited our ability to investigate *in vivo* physiological and developmental phenotypes associated with the compensatory molecular mechanism. Third, using our genetic models, we could not determine whether BCKDK phosphorylates PDC in the presence of *Pdk* family members. For that, biochemical studies of a direct interaction between BCKDK and PDC are required.

STAR★METHODS

Detailed methods are provided in the online version of this paper and include the following:

- KEY RESOURCES TABLE
- RESOURCE AVAILABILITY
  - Lead contact
  - Materials availability
  - Data and code availability
- EXPERIMENTAL MODEL AND SUBJECT DETAILS
  - Mouse lines
  - Primary cultures

SUPPLEMENTAL INFORMATION

Supplemental information can be found online at https://doi.org/10.1016/j.devcel.2021.03.007.

ACKNOWLEDGMENTS

We thank Nitzan Konstantin for expert editorial assistance, Dr. Robert Harris from Indiana University, who kindly provided us with PDK2 and PDK4 mice, Dr. Nicola Brunetti-Pierri from the Telethon Institute of Genetics and Medicine for his support and advice, Dr. Ron Rotkoff for his help with statistical analysis, Dr. Tsviya Olender for bioinformatics advice, and Neria Sharabi from the Department of Veterinary Resources for his help with mouse maintenance. Special thanks to all members of the Zelzer Laboratory for encouragement and advice. This study was supported by The David and Fela Shapell Family Center for Genetic Disorders Research, and by The Estate of Mr. and Mrs. van Adelsbergen.

AUTHOR CONTRIBUTIONS

Experiment design, L.H-Y., L.B., and E.Z.; experiments, L.H-Y., L.B., N.F., R.C.V., N.M., S.K., A.S., M.C., S.B-D., O.B., R.H-K., M.I., and S.M.; intellectual contributions, E.Z., A.E., L.H-Y., L.B., N.F., and R-C.V.; manuscript writing, L.H-Y. and E.Z. with input from all authors.

DECLARATION OF INTERESTS

The authors declare no competing interests.

Received: April 20, 2020
Revised: December 10, 2020
Accepted: March 1, 2021
Published: March 26, 2021

REFERENCES

Amarilio, R., Viukov, S.V., Sharir, A., Eshkar-Oren, I., Johnson, R.S., and Zelzer, E. (2007). HIF1alpha regulation of Sox9 is necessary to maintain differentiation of hypoxic prechondrogenic cells during early skeletogenesis. Development *134*, 3917–3928.

Aragonés, J., Fraisl, P., Baes, M., and Carmeliet, P. (2009). Oxygen sensors at the crossroad of metabolism. Cell Metab. *9*, 11–22.

Bentovim, L., Amarilio, R., and Zelzer, E. (2012). HIF1α is a central regulator of collagen hydroxylation and secretion under hypoxia during bone development. Development *139*, 4473–4483.

Bowker-Kinley, M.M., Davis, W.I., Wu, P., Harris, R.A., and Popov, K.M. (1998). Evidence for existence of tissue-specific regulation of the mammalian pyruvate dehydrogenase complex. Biochem. J. *329*, 191–196.

Broquist, H.P., and Trupin, J.S. (1966). Amino acid metabolism. Annu. Rev. Biochem. *35*, 231–274.

Caspi, R., Billington, R., Fulcher, C.A., Keseler, I.M., Kothari, A., Krummenacker, M., Latendresse, M., Midford, P.E., Ong, Q., Ong, W.K., et al. (2018). The MetaCyc database of metabolic pathways and enzymes. Nucleic Acids Res. *46*, D633–D639.

Chari, R., Mali, P., Moosburner, M., and Church, G.M. (2015). Unraveling CRISPR-Cas9 genome engineering parameters via a library- on-library approach. Nat Methods *12*, 823–826.

Crabb, D.W., and Harris, R.A. (1979). Mechanism responsible for the hypoglycemic actions of dichloroacetate and 2-chloropropionate. Arch. Biochem. Biophys. *198*, 145–152.

Doench, J.G., Fusi, N., Sullender, M., Hegde, M., Vaimberg, E.W., Donovan, K.F., Smith, I., Tothova, Z., Wilen, C., Orchard, R., et al. (2016). Optimized sgRNA design to maximize activity and minimize off-target effects of CRISPR-Cas9. Nat. Biotechnol. *34*, 184–191.

Doench, J.G., Hartenian, E., Graham, D.B., Tothova, Z., Hegde, M., Smith, I., Sullender, M., Ebert, B.L., Xavier, R.J., and Root, D.E. (2014). Rational design of highly active sgRNAs for CRISPR-Cas9-mediated gene inactivation. Nat. Biotechnol. *32*, 1262–1267.

Dunford, E.C., Herbst, E.A., Jeoung, N.H., Gittings, W., Inglis, J.G., Vandenboom, R., Leblanc, P.J., Harris, R.A., and Peters, S.J. (2011). PDH activation during in vitro muscle contractions in PDH kinase 2 knockout mice: effect of PDH kinase 1 compensation. Am. J. Physiol.Regul. Integr. Comp. Physiol. *300*, R1487–R1493.

Dunwoodie, S.L. (2009). The role of hypoxia in development of the mammalianembryo. Dev. Cell *17*, 755–773.

Eshkar-Oren, I., Viukov, S.V., Salameh, S., Krief, S., Oh, C.D., Akiyama, H., Gerber, H.P., Ferrara, N., and Zelzer, E. (2009). The forming limb skeleton serves as a signaling center for limb vasculature patterning via regulation of vegf. Development *136*, 1263–1272.

Ferriero, R., Manco, G., Lamantea, E., Nusco, E., Ferrante, M.I., Sordino, P., Stacpoole, P.W., Lee, B., Zeviani, M., and Brunetti-Pierri, N. (2013). Phenylbutyrate therapy for pyruvatedehydrogenasecomplexdeficiency and lacticacidosis. Sci. Transl. Med. *5*, 175ra31.

Garland, P.B., Newsholme, E.A., and Randle, P.J. (1964). Regulation of glucoseuptake by muscle. 9. Effects of fatty acids and ketone bodies, and of alloxan-diabetes and starvation, on pyruvate metabolism and on lactate-pyruvate and L-glycerol 3-phosphate-dihydroxyacetone phosphate concentration ratios in rat heart and rat diaphragm muscles. Biochem. J. *93*, 665–678.

Gudi, R., Bowker-Kinley, M.M., Kedishvili, N.Y., Zhao, Y., and Popov, K.M. (1995). Diversity of the pyruvate dehydrogenase kinase gene family in humans. J Biol Chem *270*, 28989–28994.

Hallmann, R., Feinberg, R.N., Latker, C.H., Sasse, J., and Risau, W. (1987). Regression of blood vessels precedes cartilage differentiation during chick limb development. Differentiation *34*, 98–105.

Harris, R.A., Bowker-Kinley, M.M., Huang, B., and Wu, P. (2002). Regulation of the activity of the pyruvate dehydrogenase complex. Adv. Enzyme Regul. *42*, 249–259.

Hsu, P.D., Scott, D.A., Weinstein, J.A., Ran, F.A., Konermann, S., Agarwala, V., Li, Y., Fine, E.J., Wu, X., Shalem, O., et al. (2013). DNA targeting specificity of RNA-guided Cas9 nucleases. Nat. Biotechnol. *31*, 827–832.

Huang, B., Gudi, R., Wu, P., Harris, R.A., Hamilton, J., and Popov, K.M. (1998). Isoenzymes of pyruvatedehydrogenasephosphatase. DNA-derived amino acid sequences, expression, and regulation. J. Biol. Chem. *273*, 17680–17688.

Jeong, J.Y., Jeoung, N.H., Park, K.G., and Lee, I.K. (2012). Transcriptional regulation of pyruvate dehydrogenase kinase. Diabetes Metab.J. *36*, 328–335.

Jeoung, N.H. (2015). Pyruvate dehydrogenase kinases: therapeutic targets for diabetes and cancers. Diabetes Metab. J. *39*, 188–197.

Jeoung, N.H., Rahimi, Y., Wu, P., Lee, W.N.P., and Harris, R.A. (2012). Fasting induces ketoacidosis and hypothermia in PDHK2/ PDHK4-double-knockout mice. Biochem. J. *443*, 829–839.

Jeoung, N.H., Wu, P., Joshi, M.A., Jaskiewicz, J., Bock, C.B., Depaoli-Roach, A.A., and Harris, R.A. (2006). Role of pyruvate dehydrogenase kinase isoenzyme 4 (PDHK4) in glucose homoeostasis during starvation. Biochem. J. *397*, 417–425.

Joshi, M.A., Jeoung, N.H., Obayashi, M., Hattab, E.M., Brocken, E.G., Liechty, E.A., Kubek, M.J., Vattem, K.M., Wek, R.C., and Harris, R.A. (2006). Impaired growth and neurologicalabnormalities in branched-chainα-keto acid dehydrogenase kinase-deficient mice. Biochem. J. *162*, 153–162.

Kim, J.W., Tchernyshyov, I., Semenza, G.L., and Dang, C.V. (2006). HIF-1-mediated expression of pyruvate dehydrogenase kinase: A metabolic switch required for cellular adaptation to hypoxia. Cell Metab. *3*, 177–185.

Kluza, J., Corazao-Rozas, P., Touil, Y., Jendoubi, M., Maire, C., Guerreschi, P., Jonneaux, A., Ballot, C., Balayssac, S., Valable, S., et al. (2012). Inactivation of the HIF-1alpha/PDK3 signaling axis drives melanoma toward mitochondrial oxidative metabolism and potentiates the therapeutic activity of pro-oxidants. Cancer Res. *72*, 5035–5047.

Koh, M.Y., and Powis, G. (2012). Passing the baton: the HIF switch. Trends Biochem. Sci. *37*, 364–372.

Kolobova, E., Tuganova, A., Boulatnikov, I., and Popov, K.M. (2001). Regulation of pyruvate dehydrogenase activity through phosphorylation at multiple sites. Biochem. J. *358*, 69–77.

Korotchkina, L.G., and Patel, M.S. (1995). Mutagenesis studies of the phosphorylation sites of recombinant human pyruvate dehydrogenase. Site-specific regulation. J. Biol. Chem. *270*, 14297–14304.

Lallemand, Y., Luria, V., Haffner-Krausz, R., and Lonai, P. (1998). Maternally expressed PGK-Cre transgene as a tool for early and uniform activation of the Cre site-specific recombinase. Transgen. Res. *7*, 105–112.

Liang, Z., Cardaci, S., Jerby, L., MacKenzie, E.D., Sciacovelli, M., Johnson, T.I., Gaude, E., King, A., Leach, J.D.G., Edrada-Ebel, R.A., et al. (2015). Fumarate induces redox-dependent senescence by modifying glutathione metabolism. Nat Commun *6*, 6001, https://doi.org/10.1038/ncomms7001.

Logan, M., Martin, J.F., Nagy, A., Lobe, C., Olson, E.N., and Tabin, C.J. (2002). Expression of Cre recombinase in the developing mouse limb bud driven by a Prxl enhancer. Genesis *33*, 77–80.

Lu, C.W., Lin, S.C., Chen, K.F., Lai, Y.Y., and Tsai, S.J. (2008). Induction of pyruvate dehydrogenase kinase-3 by hypoxia-inducible factor-1 promotes metabolic switch and drug resistance. J. Biol. Chem. *283*, 28106–28114.

Maes, C., Araldi, E., Haigh, K., Khatri, R., Van Looveren, R., Giaccia, A.J., Haigh, J.J., Carmeliet, G., and Schipani, E. (2012). VEGF-independent cell-autonomous functions of HIF-1alpha regulating oxygen consumption in fetal cartilage are critical for chondrocyte survival. J. Bone Miner. Res. *27*, 596–609.

Mcleod, M.J. (1980). Differential staining of cartilage and bone in wholemouse-fetuses by alcian blue and Alizarin Red S. Teratology *22*, 299–301.

Nishitani, S., Takehana, K., Fujitani, S., and Sonaka, I. (2005). Branched-chain amino acids improve glucose metabolism in rats with liver cirrhosis. Am. J. Physiol. Gastrointest Liver Physiol. *288*, G1292–G1300.

Oppenheim, R.D., Creek, D.J., Macrae, J.I., Modrzynska, K.K., Pino, P., Limenitakis, J., Polonais, V., Seeber, F., Barrett, M.P., Billker, O., et al. (2014). BCKDH: the missing link in api complex and mitochondrial metabolism is required for full virulence of Toxoplasma gondii and Plasmodium berghei. PLoS Pathog. *10*, e1004263.

Papandreou, I., Cairns, R.A., Fontana, L., Lim, A.L., and Denko, N.C. (2006). HIF-1 mediates adaptation to hypoxia by actively downregulating mitochondrial oxygen consumption. Cell Metab. *3*, 187–197.

Paten, B., Herrero, J., Beal, K., Fitzgerald, S., and Birney, E. (2008). Enredo and Pecan: genome-wide mammalian consistency-based multiple alignment with paralogs. Genome Res. *18*, 1814–1828.

Pettitt, S.J., Liang, Q., Rairdan, X.Y., Moran, J.L., Prosser, H.M., Beier, D.R., Lloyd, K., Bradley, A., and Skarnes, W.C. (2013). Agouti C57BL / 6N embryonicstem cells for mouse genetic resources. Nat. Methods *6*, 493–495.

Popov, K.M., Kedishvili, N.Y., Zhao, Y., Shimomura, Y., Crabb, D.W., and Harris, R.A. (1993). Primary structure of pyruvate dehydrogenase kinase establishes a new family of eukaryotic protein kinases. J. Biol. Chem. *268*, 26602–26606.

Prigione, A., Rohwer, N., Hoffmann, S., Mlody, B., Drews, K., Bukowiecki, R., Blümlein, K., Wanker, E.E., Ralser, M., Cramer, T., and Adjaye, J. (2014). HIF1alpha modulates cell fate reprogramming through early glycolytic shift and upregulation of PDK1-3 and PKM2. StemCells *32*, 364–376.

Provot, S., and Schipani, E. (2005). Molecular mechanisms of endochondral bone development. Biochem. Biophys. Res. Commun. *328*, 658–665.

Provot, S., Zinyk, D., Gunes, Y., Kathri, R., Le, Q., Kronenberg, H.M., Johnson, R.S., Longaker, M.T., Giaccia, A.J., and Schipani, E. (2007). HIF-1alpha regulates differentiation of limb bud mesenchyme and joint development. J. Cell Biol. *177*, 451–464.

Roche, T.E., and Hiromasa, Y. (2007). Pyruvate dehydrogenase kinase regulatory mechanisms and inhibition in treating diabetes, heart ischemia, and cancer. Cell. Mol. Life Sci. *64*, 830–849.

Saunier, E., Benelli, C., and Bortoli, S. (2016). The pyruvate dehydrogenase complex in cancer: an old metabolic gatekeeper regulated by new pathways and pharmacological agents. Int. J. Cancer *138*, 809–817.

Schindelin, J., Arganda-Carreras, I., Frise, E., Kaynig, V., Longair, M., Pietzsch, T., Preibisch, S., Rueden, C., Saalfeld, S., Schmid, B., et al. (2012). Fiji: an open-source platform for biological-image analysis. Nat Methods *9*, 676–682, https://doi.org/10.1038/nmeth.2019.

Schipani, E., Ryan, H.E., Didrickson, S., Kobayashi, T., Knight, M., and Johnson, R.S. (2001). Hypoxia in cartilage: HIF-1alpha is essential for chondrocyte growth arrest and survival. Genes Dev. *15*, 2865–2876.

Semba, H., Takeda, N., Isagawa, T., Sugiura, Y., Honda, K., Wake, M., Miyazawa, H., Yamaguchi, Y., Miura, M., Jenkins, D.M.R., et al. (2016). HIF-1alpha-PDK1 axis-induced active glycolysis plays an essential role in macrophage migratory capacity. Nat. Commun. *7*, 11635.

Semenza, G.L. (2001). Hypoxia-inducible factor 1: oxygen homeostasis and disease pathophysiology. Trends Mol. Med. *7*, 345–350.

Semenza, G.L. (2009). Regulation of oxygenhomeostasis by hypoxia-inducible factor 1. Physiology *24*, 97–106.

Shao, D., Villet, O., Zhang, Z., Choi, S.W., Yan, J., Ritterhoff, J., Gu, H., Djukovic, D., Christodoulou, D., Kolwicz, S.C., Jr., et al. (2018). Glucose promotes cell growth by suppressing branched-chain amino acid degradation. Nat. Commun. *9*, 2935.

Simon, M.C., and Keith, B. (2008). The role of oxygen availability in embryonic development and stem cell function. Nat.Rev.Mol. Cell Biol. *9*, 285–296.

Stacpoole, P.W. (1989). The pharmacology of dichloroacetate. Metabolism *38*, 1124–1144.

Stacpoole, P.W. (2017). Therapeutic targeting of the pyruvatedehydrogenase complex / pyruvate dehydrogenase kinase (PDC / PDK) axis in cancer. J. Natl. Cancer Inst. *109*, 1–14.

Stelzer, G., Inger, A., Olender, T., Iny-Stein, T., Dalah, I., Harel, A., Safran, M., and Lancet, D. (2009). GeneDecks: paralog hunting and gene-set distillation with GeneCards annotation. OMICS *13*, 477–487.

Stelzer, G., Rosen, N., Plaschkes, I., Zimmerman, S., Twik, M., Fishilevich, S., Stein, T.I., Nudel, R., Lieder, I., Mazor, Y., Kaplan, S., Dahary, D., Warshawsky, D., Guan-golan, Y., Kohn, A., Rappaport, N., and Safran, M. (2016). The GeneCards suite : from gene data mining to disease genome sequence analyses. Curr. Protoc. Bioinforma. *1*, 1–33.

Sugden, M.C., and Holness, M.J. (2006). Mechanisms underlying regulation of the expression and activities of the mammalian pyruvate dehydrogenase kinases. Arch. Physiol. Biochem. *112*, 139–149.

Szklarczyk, D., Morris, J.H., Cook, H., Kuhn, M., Wyder, S., Simonovic, M., Santos, A., Doncheva, N.T., Roth, A., Bork, P., et al. (2017). The STRING database in 2017: quality-controlled protein-protein association networks, made broadly accessible. Nucleic Acids Res. *45*, D362–D368.

Tennessen, J.M., Bertagnolli, N.M., Evans, J., Sieber, M.H., Cox, J., and Thummel, C.S. (2014). Coordinated metabolictransitions during Drosophila embryogenesis and the onset of aerobicglycolysis. G3 (Bethesda) *4*, 839–850.

Tracy, B.Y., Flora, C.L., and Reed, L.J. (1968). a-keto acid dehydrogenase complexes, x. regulation of the activity of the pyruvate dehydrogenase complex from beef kidney mitochondria by phosphorylation and dephosphorylation. Proc. Natl. Acad. Sci. USA *62*, 234–241.

Wang, H., Yang, H., Shivalila, C.S., Dawlaty, M.M., Cheng, A.W., Zhang, F., and Jaenisch, R. (2013). One-step generation of mice carrying mutations in multiple genes by CRISPR/Cas-mediated genome engineering. Cell *153*, 910–918.

Weissgerber, T.L., and Wolfe, L.A. (2006). Physiological adaptation in early human pregnancy: adaptation to balance maternal-fetal demands. Appl. Physiol. Nutr. Metab. *31*, 1–11.

Wieland, O.H. (1983). The mammalian pyruvate dehydrogenase complex: structure and regulation. Rev. Physiol. Biochem. Pharmacol. *96*, 123–170.

Wynn, R.M., Chuang, J.L., Cote, C.D., and Chuang, D.T. (2000). Tetrameric assembly and conservation in the ATP-binding domain of rat Branched-chain alpha-keto acid dehydrogenase kinase. J. Biol. Chem. *275*, 30512–30519.

Xu, H., Xiao, T., Chen, C.H., Li, W., Meyer, C.A., Wu, Q., Wu, D., Cong, L., Zhang, F., Liu, J.S., et al. (2015). Sequence determinants of improved CRISPR sgRNA design. Genome Res. *25*, 1147–1157.

Zhang, S., Zeng, X., Ren, M., Mao, X., and Qiao, S. (2017). Novel metabolic and physiological functions of branched chain amino acids: a review. J. Anim. Sci. Biotechnol. *8*, 10.

Zhou, M., Lu, G., Gao, C., Wang, Y., and Sun, H. (2012). Tissue-specific and nutrient regulation of the Branched-chain alpha-keto acid dehydrogenase-phosphatase, Protein phosphatase 2cm (PP2Cm). J. Biol. Chem. *287*, 23397–23406.

STAR★METHODS

KEY RESOURCES TABLE

REAGENT or RESOURCE	SOURCE	IDENTIFIER
Antibodies		
Rabbit anti-PDK1	Abcam	Cat#AB202468
Rabbit anti-PDK2	Abgent	Cat#AP7039b
Rabbit anti-PDK3	Abgent	Cat#AP14274b
Rabbit anti-PDK4	Abgent	Cat#AP7041b
Rabbit anti- BCKDK	Abcam	Cat#AB111716
Mouse anti-PDHe1	Abcam	Cat#AB110334
Rabbit anti-PDHe1α S300	Calbiochem	Cat#AP1064
Rabbit anti-PDHe1α S232	Calbiochem	Cat#AP1063
Rabbit anti-PDHE1α S293	Calbiochem	Cat#AP1062
Mouse anti-GAPDH	Ambion	Cat#AM4300
Goat anti-mouse HRP	Abcam	Cat#AB98808
Donkey anti-rabbit HRP	Jackson Immuno Research laboratory	Cat#711-035-152
Bacterial and Virus Strains		
Ad5CMVCREeGFP	Gene Transfer Vector Core, University of Iowa	N/A
Ad5CMVeGFP	Gene Transfer Vector Core, University of Iowa	N/A
Chemicals, Peptides, and Recombinant Proteins		
PBS	Biological Industries	Cat#02-023-1A
DMEM 4500 mg/ml glucose	Thermo Fisher Scientific	Cat#41965-039
DMEM free	Biological Industries	Cat#
Trypsin EDTA 0.25%	Biological Industries	Cat#03-050-1B
Collagenase type V	Sigma Aldrich	Cat# C9263
Penicillin-streptomycin solution	Biological Industries	Cat#03-031-1B
Fetal bovine serum	Biological Industries	Cat#04-007-1A
L-glutamine	Biological Industries	Cat#03-020-1B
[13-C]Sodium pyruvate	Sigma Aldrich	Cat#490-717
Sodium pyruvate	Biological Industries	Cat#03-042-1B
EDTA	Mallinckrodt-Baker	Cat#8993-01
Ethanol ABS	Gadot-Group	Cat#830000054
Paraformaldehyde	Sigma Aldrich	Cat#441244
EGTA	Sigma Aldrich	Cat#3E4378
Deoxycholate	Fluka BioChemika	30970
IGEPAL CA-630 (NP-40)	Sigma Aldrich	Cat#I8896
Magnesium chloride	EMD- Merck Millipore	Cat#105833
Potassium ferricyanide	Sigma	P8131
X-gal	Inalco Pharmaceuticals	Cat#1758-0300
Mayer's modified hematoxylin (Gill III)	Sigma Aldrich	Cat#H9627-25G
Xylen	Bio-lab	Cat#242505
Alcian Blue	Sigma Aldrich	A3157
Alizarin Red S	Sigma Aldrich	Cat#A5533
Potassium hydroxide	Mallinckrodt-Baker	Cat#6984-04
Sodium chloride	Bio-lab	Cat#19030501

(*Continued on next page*)

Continued

REAGENT or RESOURCE	SOURCE	IDENTIFIER
Sodium dodecyl sulfate	Sigma Aldrich	Cat#L4509-250G
Tris	MP-biomedicals	Cat#04819620
Tris-HCl	Bio-lab	Cat#002083232300
Glycerol	Bio-lab	Cat#7120201
β-mercaptoethanol	Sigma Aldrich	Cat#M7522
Bromophenol blue	Sigma Aldrich	114391
Nitrocellulose membrane	Whatmann	Cat#10401383
Ponceau	Sigma	Cat#P7170
Milk powder (skim)	Tnuva	
TWEEN-20	Sigma Aldrich	Cat#P1379
BSA fraction V	Sigma Aldrich	Cat#A7906
Sodium azide	Sigma	Cat#S2002
Methanol	Bio-lab	Cat#136805
miniComplete Protease inhibitor	Roche	Cat#11836153001
PhosStop -Phosphatase inhibitor	Roche	Cat# PHOSS-RO
MEM-non-essentialamino acid	Biological Industries	Cat#01-340-1B
miniCollect tube	Greiner bio-one	Cat#A170734Y
Absolute Blue qPCR SYBR Green ROX Mix	Thermo Fisher Scientific	Cat#AB-4162/B
Critical Commercial Assays		
PDH activity assay	Sigma	Cat#MAK-183
RNeasy microkit	Qiagen	Cat#74034
High Capacity Reverse Transcription Kit	Applied Biosystems	Cat#4368814
BCA assaykit	Cyanagen	Cat#9470BCAINCBSA
EZ-ECL Chemiluminescence detection kit	Biological Industries	20-500-120
Deposited Data		
Raw and analyzeddata	This paper	N/A
Experimental Models: Cell Lines		
Primary chondrocyte	This paper	N/A
Primary mouseembryonicfibroblast	This paper	N/A
Experimental Models: Organisms/Strains		
Mouse (Mus musculus): *Pdk2* KO	Dunford et al., 2011	MGI:1343087
Mouse: *Pdk4* KO	Jeoung et al., 2006	MGI:1351481
Mouse: *Pdk1* KO, floxed-*Pdk1*, *Pdk1-lacZ* (*Pdk1*^{tm1a}(EUCOMM)^{Hmgu})	EUCOMM This paper	N/A
Mouse: *Pdk3* KO	This paper	N/A
Mouse: *Bckdk* KO	This paper	N/A
Mouse: *Prx1-Cre*	Logan et al., 2002	MGI:2450929
Mouse: *Pgk*-Cre	Lallemand et al.,1998	N/A
Mouse: *Rosa26-FLPe*	Jackson laboratory	016226
Oligonucleotides		
gRNA: *Pdk3*5'-CGGGTTGGGGAGGTCTAGAG-3'	This paper	N/A
gRNA: *Pdk3*5'-ATTCCGTGAGAAGCTCCGGG-3'	This paper	N/A
gRNA: *Bckdk*5'-CCCGCGCGATGTTACAGCCG-3'	This paper	N/A
gRNA: *Bckdk5*'-CTCTACATGGTGTGTATCGG-3'	This paper	N/A
Genotype primer: *Pdk1* KO / *Pdk1-lacZ* forward TATTTGTGTCTAGTCAATGACTTGGG	EUCOMM	N/A
Genotype primer: *Pdk1* KO / *Pdk1-lacZ* reverse CAACGGGTTCTTCTGTTAGTCC	EUCOMM	N/A
Genotype primer: *Pdk1*floxed forward TATTTGTGTCTAGTCAATGACTTGGG	EUCOMM	N/A

(*Continued on next page*)

Continued

REAGENT or RESOURCE	SOURCE	IDENTIFIER
Genotype primer: *Pdk1*floxed reverse AACGGTACATTTACCATAGTGAGAGG	EUCOMM	N/A
Genotype primer: *Pdk2* forward TAATCTTGACCCTGGACCAAGG	Dunford et al., 2011	N/A
Genotype primer: *Pdk2* reverse WT TTGATCTCTTTCATGATGTTGG	Dunford et al., 2011	N/A
Genotype primer: *Pdk2* reverse KO CGCTTTTCTGGATTCATCGACTGTGGC	Dunford et al., 2011	N/A
Genotype primer: *Pdk3* forward TTGGAAGCGTAGGACCACAT	This paper	N/A
Genotype primer: *Pdk3* reverse WT CCGCGACACCTACACAAGTA	This paper	N/A
Genotype primer: *Pdk3* reverse KO TTCAGGAGAGTGCGGTTTGA	This paper	N/A
Genotype primer: *Pdk4* forward CTCGAGCGAACACCAATGCACGCTC	Jeoung et al., 2006	N/A
Genotype primer: *Pdk4* reverse WT GGTGCTCGAGCCTGGGTGAAGG	Jeoung et al., 2006	N/A
Genotype primer: *Pdk4*reverse KO CGCTTTTCTGGATTCATCGACTGTGGC	Jeoung et al., 2006	N/A
Genotype primer: *Bckdk* forward GGAAGACAGGAGCCCTCATAAA	This paper	N/A
Genotype primer: *Bckdk* reverse TCTCTGCTGCCACATCAATG	This paper	N/A
qPCR primers - see table in STAR Methods	This paper	N/A
Software and Algorithms		
StepOnePlus software version 2.2		N/A
Metacyc	Caspi et al., 2018	N/A
Qual Browser	Thermo Fisher Scientific	N/A
R		N/A
Fiji	Schindelin et al., 2012	https://imagej.net/Fiji

RESOURCE AVAILABILITY

Lead contact

Further information and requests for resources and reagents should be directed to and will be fulfilled by the Lead Contact, Elazar Zelzer (Eli.zelzer@weizmann.ac.il).

Materials availability

All unique reagents generated in this study are available from the Lead Contact.

Data and code availability

The data reported in this study are available from the Lead Contact.

EXPERIMENTAL MODEL AND SUBJECT DETAILS

Mouse lines

Pdk2 KO (Dunford et al., 2011) and *Pdk4* KO mice (Jeoung et al., 2006) were previously described. The *Pdk1* KO, floxed-*Pdk1* and *Pdk1-lacZ* mice were generated as follows: Embryonic stem cells with a gene trap insertion (KO-first allele) in the *Pdk1* gene were obtained from the European Conditional Mouse Mutagenesis program (EUCOMM) (Pettitt et al., 2013). *Pdk1* KO mice were crossed with PGK-Cre mice (Lallemand et al., 1998) to generate the null *Pdk1-lacZ* mice. Alternatively, *Pdk1* KO mice were crossed with *Rosa26-FLPe* mice (Jackson laboratory, 016226) to generate the floxed-*Pdk1* mice. Genotyping of *Pdk1* KO, *Pdk1-lacZ* and floxed-*Pdk1* mice was performed by PCR (primer sequences are shown in Key Resource Table).

Generation of double and triple KO combinations of *Pdk1*, *Pdk2* and *Pdk4* was done by strain breeding. *Pdk3* KO and *Bckdk* KO were generated as follows: Cas9 plasmid and plasmids encoding guide RNAs were designed and optimized for the best guides using several CRISPR designing tools, including the MIT CRISPR design tool (Hsu et al., 2013) and sgRNA Designer, Rule Sets 1 and 2 (Doench et al., 2016, 2014), in both the original sites and later in the Benchling implementations (www.benchling.com), SSC(Xu et al., 2015), and sgRNAscorer (Chari et al., 2015), in their websites. The following oligos were used for construction of gRNA: Pdk3: 5'-CGGGTTGGGGAGGTCTAGAG-3' (upstream of the putative TSS) and 5'-ATTCCGTGAGAAGCTCCGGG-3' (downstream of the ATG in the first exon), total deletion of 560 bp(location X:93831603-93832603). For Bckdk: 5'-CCCGCGCGATGTTA CAGCCG-3' (an upstream guide around the TSS) and 5'-CTCTACATGGTGTGTATCGG-3' (downstream of the ATG in the second exon), total deletion of 884bp (location chr7:127903907-127905206). In vitro transcribed Cas9 RNA (100 ng ml) and sgRNA (50 ng ml) were injected into one-cell stage fertilized embryos isolated from superovulated *Prx1-Cre*;*Pdk1*$^{flox/-}$*Pdk2*$^{-/-}$*Pdk4*$^{-/-}$ or *Prx1-Cre*;*Pdk1*$^{flox/-}$*Pdk2*$^{-/-}$*Pdk3*$^{-/-}$*Pdk4*$^{-/-}$ mice mated with males of the same mutation to generate *Pdk* total KO or *Pdk* cKO-*Bckdk* KO mice, respectively. Injected embryos were transferred into the oviducts of pseudopregnant ICR females as previously described

(Wang et al., 2013). Genomic DNA from treated embryos was analyzed by PCR primers designed to verify the deleted sequence of each gene; primer sequences are shown in Table S1.

Staff and veterinary personnel monitored all mouse strains daily for health and activity. Mice were given ad libitum access to water and standard mouse chow with 12-hr light/dark cycles. All animal procedures were approved by the Institutional Animal Care and Use Committee and performed in strict adherence to Weizmann Institute Animal Care and Use guidelines, following the NIH, European Commission, and Israeli guidelines. In all timed pregnancies, plug date was defined as E0.5. For harvesting of embryos, timed-pregnant female mice were sacrificed by CO_2 intoxication. The gravid uterus was dissected out and suspended in a bath of ice-cold PBS and the embryos were harvested. Tail genomic DNA was used for genotyping. All procedures and treatments are described as in Method Details. None of the mice was involved in any previous procedures prior to the study.

Primary cultures

For chondrocyte primary culture, hindlimb tibiofemoral growth plates of E17.5 *Pdk1* KO, *Prx1-Cre*;*Pdk1*$^{flox/-}$*Pdk2*$^{-/-}$*Pdk3*$^{-/-}$*Pdk4*$^{-/-}$ or WT embryos were dissected and soft tissue, skin and particularly muscles were removed. The growth plates were dissected and placed in DMEM 4500 mg/l glucose (Thermofisher) with 1% pen-strep solution (Biological Industries). Growth plates were digested in trypsin containing 0.25% EDTA (Biological Industries) for 30 minutes at 37°C and in 1 mg/ml collagenase type V (Sigma) in DMEM 4500 mg/l glucose with 1% pen-strep solution for 2 hours. Chondrocytes were plated at a density of 125x10^3 cells/ml and grown under normoxia in monolayer cultures in high glucose DMEM supplemented with 10% fetal bovine serum (FBS, Biological Industries) and 1% pen-strep solution for 5 days until confluence (>90%).

Mouse embryonic fibroblasts (MEFs) were extracted from E12.5-E14.5 *Pdk* total KO, *Prx1-Cre*;*Pdk1*$^{flox/flox}$*Pdk2*$^{-/-}$*Pdk3*$^{-/-}$*Pdk4*$^{-/-}$ or ICR (WT) embryos, and cultured under normoxic conditions in DMEM (Gibco), 20% fetal calf serum, 1% L-glutamine,1% MEM-non-essential amino acid (Biological Industries), 1% penicillin/ streptavidin and sodium pyruvate. At passage 3 or 4, cells were harvested for either qRT-PCR, western blot analysis or viral infection. All procedures and treatments are described in Method Details.

METHOD DETAILS

Viral infection

For adeno-viral infection, MEFs were infected with 350 viral particles/cell of Ad5CMVeGFP or Ad5CMVCre-eGFP virus (Gene Transfer Vector Core, University of Iowa). MEFs were plated at a density of 500x10^3 cells in 6-cm plates with the same growth medium containing the AdCMV virus for 24 h, when medium was added. Medium was replaced after 48 h and cells were harvested for western blot analysis or metabolic LC-MS/MS analysis 5 days post-infection. During all experiments, medium was changed daily.

Histology

For hematoxylin and eosin staining (H&E), embryos were fixed overnight in 4% paraformaldehyde (PFA) -phosphate-buffered saline (PBS), decalcified in a solution containing equal parts of 0.5 M ethylenediaminetetraacetic acid (EDTA; pH 7.4) and 4% PFA in PBS overnight, dehydrated to 100% ethanol, embedded in paraffin and sectioned at a thickness of 7 μm. For pathological examination, whole body embryo sections were made. H&E staining was performed following standard protocols.

X-gal staining

Whole-mount X-gal staining was performed as described previously (Eshkar-Oren etal., 2009). In short, freshly dissected tissue was fixed in 4% PFA/PBS, rinsed in a solution containing 5 mM EGTA, 0.01% deoxycholate, 0.02% NP40 and 2 mM $MgCl_2$, and then stained in a solution containing 5 mM $K_3Fe(CN)_6$, 5 mM EGTA, 0.01% deoxycholate, 0.02% NP40, 2 mM $MgCl_2$ and 1 mg/ml X-gal. The tissue was cleared in 0.3% KOH for better visualization.

Skeletal preparation

Cartilage and bones were visualized using staining with Alcian Blue and Alizarin Red S (Sigma) as previously described with modifications (Mcleod, 1980). In short, after sacrifice, whole embryo or newborn pups were placed in a tube with 70% ethanol for semi-fixation, 4 °C, overnight, before removal of skin and internal organs.

For cartilage and mineral staining, embryo/ pups were embedded with skeleton preparation solution (0.18% alcian blue in 70% ethanol- 1.5 volume; 0.12% alizarin red S in 95% ethanol – l volume; acetic acid –1.25 volume; 70% ethanol -6 volumes) covered with foil at room temperature (RT) rocking, overnight. For clearing, stained embryos/ pups were rinsed with DDW, and washed with decreasing percentage of KOH (in DDW) –3.6%, 1.8%, 0.9%, 0.3%, 30 min each step (times may vary according to sample age). For final clearing, KOH was replaced with 0.3%KOH-glycerol (50:50) at RT gently rocking, overnight, and stored in 100% glycerol at RT.

Glucose, glutamine, glutamate and lactate measurements

Chondrocytes were plated as described above. Upon reaching 90% confluence, cells were washed and incubated in a glucose- and glutamine-free DMEM medium supplemented with 10% dialyzed serum, 4 mM L-glutamine 10mM glucose, for 12 h. Subsequently, 500 μL medium from the cell culture was collected, briefly centrifuged and directly injected into the Nova chemical analyzer. Background metabolite measurements from cell-free culture were subtracted, and results were normalized to cell number.

RNA isolation and quantitative real-time (qRT-) PCR

Total RNA was purified from either MEFs or chondrocyte primary culture using the RNeasy Kit (Qiagen). Reverse transcription was performed with High Capacity Reverse Transcription Kit (Applied Biosystems) according to the manufacturer's protocol. qRT-PCR was performed using Fast SYBR Green master mix (Applied Biosystems) on the StepOnePlus machine (Applied Biosystems). Values were calculated using the StepOne software version 2.2, according to the relative standard curve method. Ctvalues were normalized to TATA-box binding protein (Tbp) or 18S rRNA. Statistical significance was determined by Student's t-test as $P<0.05$.

Primer:	Sequence:
Pdk1- forward	CGTACAGCTGGTGCAAAGTT
Pdk1- reverse	ATTGTGCCGGTTTCTGATCC
Pdk2- forward	GCGCTGTTGAAGAATGCGT
Pdk2- reverse	GCCGGAGGAAAGTGAATGAC
Pdk4- forward	CAGGGAGGTCGAGCTGTTC
Pdk4- reverse	AGGACGTTCTTTCACAGGCA
Pdk3- forward	TCCTGGACTTCGGAAGGGATA
Pdk3- reverse	TCATGGTGTTAGCCAGTCGC
Bckdk-forward	AGACTTCCCTCCGATCAAGGA
Bckdk-reverse	TTTCCGGCTCTCACGAAGAC
Tbp- forward	GCAGCCTCAGTACAGCAATCAACA
Tbp- reverse	GGTGCAGTGGTCAGAGTTTGAGAA
18S- forward	GTAACCCGTTGAACCCCATT
18S- reverse	CCATCCAATCGGTAGTAGCG

Western blot analysis

For western blotting, protein was extracted using RIPA (150 mM NaCl, 1% NP40, 0.5% Deoxycholate, 0.1% sodium dodecyl sulfate (SDS), 50 mM Tris (pH 8.0)) supplemented with PI(1:100) and phosphatase inhibitors (1:20), homogenized using Motor Cordless (Kimble) and centrifuged at 10,000 rpm, 4 °C for 10 min. Supernatant was collected and used for the following procedures. In the case of heart, kidney and lungs extracts were supplemented by sonication (SONICS, Vibra-Cell™) post-homogenization. Protein concentration was determined by Pierce protein BCA assay kit (Cyanagen). 40 μg protein extracts were denatured by boiling in × 5 sample buffer (60 mM Tris-HCl (pH 6.8), 25% glycerol, 2% SDS, 14.4 mM β-mercaptoethanol, 0.1% bromophenol blue) for 5 min, resolved by 10% SDS-PAGE, 100–120 V, for 70 min and transferred to nitrocellulose membrane (Whatmann, 10401383) at 250 mA for 70 min. Membranes were stained with Ponceau (Sigma-Aldrich, P7170) and blocked for 60 min at RT with 5% milk-0.05% TWEEN-20. Next, membrane was incubated rocking with primary antibodies in Antibody solution (5% BSA fraction V, 5% sodium azide, 0.05% PBST) overnight at 4 °C. Membranes were washed 3 × 5 min at RT with 0.05% PBST and incubated for 60 min with horseradish peroxidase (HRP)-conjugated secondary antibodies. Membranes were washed 3 × 5 min, processed with EZ-ECL Chemiluminescence detection kit for HRP (Biological Industries, 20-500-120) and visualized by ImageQuant™ LAS 4000 (GE Healthcare Life Sciences). Densitometry values were normalized to GAPDH in the same lane.

PDH activity assay

PDH Activity Assay Kit (Sigma) was used according to the manufacturer's instruction. In short, protein was extracted from ~10^6 MEF cells, homogenized using Motor Cordless (Kimble) in 100 μL of ice-cold PDH Assay Buffer and centrifuged at 10,000 rpm, 4 °C for 5 min. Supernatant was collected and used immediately (20 μl per well). Colorimetric reads were done by Infinite® 200 PRO NanoQuant (Tecan); samples were normalized to cell count.

Ketone bodies and glucose blood levels measurements

3-beta-hydroxybutyrate (3HB), a prevalent ketone body, and glucose were measured by Freestyle Optium Neo machine (GeffenMedical) and Performa blood meter (ACCU-CHECK®), respectively, using a drop of blood from P1 *Pdk* total KO pups.

Bioinformatic analysis of potential *Pdk* paralogs

Paralog analysis for *Pdk1* was performed using GeneCards Suite - GenesLikeMe tool (GeneCards Suite) (https://www.genecards.org/) for related genes. Total score for best 100 functional partners was calculated using an algorithm combining sequence, domain, super pathways, expression pattern, phenotypes, compounds and gene ontology similarities (Stelzer et al., 2009).

Protein-protein interaction analysis for BCKDK was preformed using STRING: functional protein association networks (https://string-db.org/). Calculation of predicted functional partners score was done based on experimentally or database known

interactions, predicted neighborhood, fusion and gene co-occurrence, textmining, co-expression, and protein homology (Szklarczyk et al., 2017).

Mendelian ratio analysis

All genotype distribution were analyzed by monitoring colony progeny (4-6 months) or embryos from experiments, using tail PCR genotyping followed by Chi-square test. n values are given in the figure legends.

Metabolite extraction

For serum metabolite composition analysis, total blood volume (about 50 μl) from P1 *Pdk* total KO pups were collected into serum separation tubes (MiniCollect Tubes, greiner bio-one) and centrifuged at 1000 rpm for 5 min at RT. Serum was collected and immediately frozen in safe-lock Eppendorf tubes in liquid nitrogen. For labeled metabolites, MEF primary culture were grown and infected as described. 5 days post-infection growth medium was removed, cells were washed with pre-warmed PBS and medium was replaced with DMEM free of L-Glutamine, Glucose and Sodium Pyruvate (Biological Industries) supplemented with 2.5mM glucose, 2.5 mM [3-^{13}C]pyruvate, 2 mM l-glutamine and MEM-eagle non-essential amino acids X1, and incubated at 37 °C, for 1.5 h. Then, medium was removed and cells were washed twice with 2 ml 0.9% ice-cold saline. Cells were scraped from plates with 500 μl of ice-cold methanol:DDW (1:1, v:v) containing C13 and N15 labeled amino acid mix (Sigma-Aldrich) as internal standards; a total volume of 1000 μl from 2X plates per sample (about 2X10^6 cells) were collected into safe-lock Eppendorf tubes. Samples underwent three freeze-thaw cycles in liquid nitrogen -37°C bath sonicated in ice-bath for 30 min, and vortexed each 10 min. Then, the samples were centrifuged for 15 min at maximum speed (14000 rpm) at 4°C. Supernatant (800 μL) was transferred to another Eppendorf tube, dried for 1 h in speedvac and lyophilized. The dry pellet was re-suspended in 100 μL methanol:DDW (1:1, v:v) and centrifuged twice for 15 min at maximum speed (14000 rpm) at 4°C. Then, the supernatant was transferred into vials for injection.

LC-MS polar metabolites analysis

Metabolic profiling of polar phase was done as described by Liang et al. (2015) with minor modifications. Briefly, analysis was performed using Acquity I class UPLC System (Waters) combined with Exactive™ Plus Orbitrap Mass Spectrometer (Thermo Scientific™), which was operated in a negative ionization mode. The LC separation was done using the SeQuant Zic-pHilic (150 mm × 2.1 mm) with the SeQuant guard column (20 mm × 2.1 mm) (Merck). The Mobile phase A consisted of acetonitrile and Mobile phase B consisted of 20 mM ammonium carbonate plus 0.1% ammonia hydroxide in water. The flow rate was kept at 200 μl min−1 and gradient as follow: 0 -2 min 75% of B, 17 min 12.5% of B, 17.1 min 25% of B, 19 min 25% of B, 19.1 min 75% of B, 19 min 75% of B.

Polar metabolites data analysis

The data were collected using Xcalibur 4.15 and processed using Qual Browser (Thermo Fisher Scientific™). Compounds were identified by retention time and fragments and were verified using in-house mass spectra library. Metabolic pathway analysis was done using Metacyc database (Caspi et al., 2018).

QUANTIFICATION AND STATISTICAL ANALYSIS

Statistical analyses of qRT-PCR, chondrocyte metabolites and ketone-glucose blood levels were performed with Excel using unpaired two-tailed Student's t-test. PDH activity assay and metabolic profiling statistics were done using R ANOVA multiple comparison analysis. Statistical significance is denoted by asterisks ($P<0.05$ [*], $P< 0.01$ [**], and $P< 0.0001$ [***]. The data are presented as mean±SD. All statistical details, including n values, are given in the figures and figure legends.